The Astrophysical Journal, 836:88 (19pp), 2017 February 10 https://doi.org/10.3847/1538-4357/836/1/88

Continuum Foreground Polarization and Na I Absorption in Type Ia SNe*

P. Zelaya[1,2], A. Clocchiatti[1,2], D. Baade[3], P. Höflich[4], J. Maund[5], F. Patat[3], J. R. Quinn[2], E. Reilly[5], L. Wang[6], J. C. Wheeler[7], F. Förster[1,8], and S. González-Gaitán[1,8]
[1] MAS—Millennium Institute of Astrophysics, Casilla 36-D,7591245, Santiago, Chile; pazelaya@astro.puc.cl
[2] Instituto de Astrofísica, Pontificia Universidad Católica de Chile, Casilla 306, Santiago 22, Chile
[3] ESO—European Organization for Astronomical Research in the Southern Hemisphere, Karl-Schwarzschild-Str.2, D-85748 Garching b. München, Germany
[4] Department of Physics, Florida State University, Tallahassee, FL 32306-4350, USA
[5] Department of Physics and Astronomy, University of Sheffield, Hicks Building, Hounsfield Road, Sheffield, S3 7RH, UK
[6] Department of Physics, Texas A&M University, College Station, TX 77843-4242, USA
[7] Department of Astronomy and McDonald Observatory, The University of Texas at Austin, 1 University Station, C1400, Austin, TX 78712, USA
[8] Departamento de Astronomía, Universidad de Chile, Casilla 36-D, Santiago, Chile
Received 2016 June 5; revised 2016 December 28; accepted 2017 January 12; published 2017 February 10

Abstract

We present a study of the continuum polarization over the 400–600 nm range of 19 SNe Ia obtained with FORS at the VLT. We separate them into those that show Na I D lines at the velocity of their hosts and those that do not. Continuum polarization of the sodium sample near maximum light displays a broad range of values, from extremely polarized cases like SN 2006X to almost unpolarized ones like SN 2011ae. The non-sodium sample shows, typically, smaller polarization values. The continuum polarization of the sodium sample in the 400–600 nm range is linear with wavelength and can be characterized by the mean polarization ($P_{\rm mean}$). Its values span a wide range and show a linear correlation with color, color excess, and extinction in the visual band. Larger dispersion correlations were found with the equivalent width of the Na I D and Ca II H and K lines, and also a noisy relation between $P_{\rm mean}$ and R_V, the ratio of total to selective extinction. Redder SNe show stronger continuum polarization, with larger color excesses and extinctions. We also confirm that high continuum polarization is associated with small values of R_V. The correlation between extinction and polarization—and polarization angles—suggest that the dominant fraction of dust polarization is imprinted in interstellar regions of the host galaxies. We show that Na I D lines from foreground matter in the SN host are usually associated with non-galactic ISM, challenging the typical assumptions in foreground interstellar polarization models.

Key words: circumstellar matter – dust, extinction – supernovae: general

1. Introduction

Since the proposal of Wheeler & Hansen (1971), SNe Ia have been firmly established as the result of the thermonuclear runaway of a carbon–oxygen (CO) white dwarf (WD) that has accreted matter from a donor star until the Chandrasekhar mass limit has been reached. Significant features of the progenitor system and the explosion, however, remain unexplained. Questions such as what the companion star is, how fast the mass is accreted, at what mass the CO WD explodes, how the explosion is triggered, and how it burns its nuclear fuel, are still subject to debate. There are two popular progenitor models: the single degenerate (SD) model (Whelan & Iben 1973; Nomoto 1982; Iben & Tutukov 1996), where a WD accretes mass from a non-degenerate star, and the double degenerate (DD) model (Iben & Tutukov 1984; Webbink 1984; Pakmor et al. 2012), where two CO WDs violently merge. Both SD and DD scenarios have collected favorable, albeit at times contradictory, observational evidence.

Since the SD and DD models imply different circumstellar environments, observations with the potential of diagnosing the local neighborhood of the SNe have the potential of distinguishing between the two progenitor channels. The presence of variable components of the Na I D narrow absorption lines in some SNe, like SNe 1999cl, 2006X, and 2007le (Blondin et al. 2009; Patat et al. 2009; Simon et al. 2009 respectively), the statistics of the velocity shifts of these lines (Sternberg et al. 2011; Maguire et al. 2013), studies of the circumstellar matter (CSM) in supernova remnants like *Kepler* (Burkey et al. 2013), and the blue light excess found in SN 2012cg by Marion et al. (2016) have all been linked to the SD scenario, and all suggest that the presence of a rich CSM is associated with an evolving, non-degenerate, companion star. On the other hand, the extremely near SN 2011fe, which was first observed just a couple of hours after explosion, puts strong constraints on the luminosity and mass of the companion. A normal non-degenerate star is practically ruled out in favor of the DD scenario (Li et al. 2011; Pakmor et al. 2012).

Finally, the entire connection of variable Na I D lines with the SD scenario has been brought into question by Soker (2014). He proposes that the variability of the Na I D lines results from gas being adsorbed by, or de-adsorbed from, dust grains.

Spectropolarimetry allows for new insights into the problem of the progenitor systems because it provides information on the SNe and the material in their lines of sight that is not available in the usual intensity versus wavelength observations. As routine spectropolarimetry of SNe Ia goes through its second decade, it is fairly safe to say that, within the constraints of the signal-to-noise ratio, the observation of appreciable continuum polarization in normal events is rare. Although there have been some detections, most of them can be associated with peculiar SNe or comfortably explained as the result of

* Based on observations made with ESO Telescopes at the Paranal Observatory under programs 068.D-0571(A), 069.D-0438(A), 070.D-0111(A), 076.D-0178(A), 079.D-0090(A), 080.D-0108(A), 081.D-0558(A), 085.D-0731(A), and 086.D-0262(A). Also based on observations collected at the German-Spanish Astronomical Center, Calar Alto (Spain).

typical foreground interstellar polarization (ISP). Howell et al. (2001) found a peak of 0.8% intrinsic continuum polarization for SN 1999by, higher than the <0.4% expected for normal Type Ia's (Wang & Wheeler 2008). For this subluminous event, the polarization peaks in the red side of the spectrum and decreases to the blue, as predicted by the model of Wang et al. (1997). Additionally Patat et al. (2012) found intrinsic continuum polarization ~0.7% for SN 2005ke, also increasing from blue to red wavelengths. SN 2005hk showed more typical lower levels of intrinsic continuum polarization, 0.36% and 0.18%, as reported by Chornock et al. (2006) and Maund et al. (2010a), respectively. These three SNe were classified as peculiar: SN 1999by and SN 2005ke are subluminous events and SN 2005hk corresponds to a 2002cx-like SNe (Li et al. 2003). From the study of a sample of four SNe, Leonard et al. (2005) suggested that normal, and perhaps overluminous, SNe displayed weak continuum polarization ($\lesssim$0.4%) and that subluminous ones showed larger values, although still modest (~0.8%).

SN 2006X is particularly noteworthy in this context. Patat et al. (2009) found that it had a strong continuum polarization, which rose sharply toward the blue and remained constant over the 49 days covered by the observations. The atypical dependence with wavelength suggested an unusual origin for the polarization, but the constancy in time indicated that it was not intrinsic to the SN. The wavelength dependence could not be successfully matched by a Serkowski law (Serkowski et al. 1975), which incorporates the relation between a wavelength of maximum polarization, $\lambda_{\rm max}$, and a "constant" K found by Whittet et al. (1992), which is generally used to describe the polarization of the Milky Way interstellar medium (ISM). In spite of this, the polarization was reasonably well-aligned with a spiral arm of the host at the projected position of the SN. The polarization of light transmitted through the ISM is known to align parallel to the magnetic field lines (e.g., Mathewson & Ford 1970). This is explained as the effect of extinction by elongated dust grains aligned with the interstellar magnetic field by the paramagnetic relaxation mechanism of Davis & Greenstein (1951), which could be greatly accelerated by radiative torques and possibly slowed down by the active formation of hydrogen molecules on the grain surface (Draine & Weingartner 1997). Magnetic fields, in addition, are known to align with large-scale structures of galaxies, like spiral arms (e.g., Mathewson & Ford 1970; Scarrott et al. 1987). Accordingly, Patat et al. (2009) interpreted the continuum polarization of SN 2006X as foreground polarization of interstellar origin, even though it had a very peculiar wavelength dependence. They suggested that this peculiarity resulted from abnormal dust and related it to the peculiar reddening laws found for many SNe Ia (Wang et al. 2006, 2009; Folatelli et al. 2010). In addition, high-resolution spectroscopy for this SN showed that the bulk of reddening came from a cold molecular cloud, which strengthens the idea of unusual dust in that particular region. Patat et al. (2009) found that the steep rise to the blue of the polarization spectrum was reasonably well matched by a Serkowski law with a very small $\lambda_{\rm max}$ and $K \sim 1.1$, a pair of values that does not satisfy the relation of Whittet et al. (1992). Because of these odd parameters, Patat et al. (2009) chose to model the continuum polarization with a cubic function to represent the ISP. The procedure is sensible but highlights how difficult it is to uncover any continuum polarization intrinsic to the SN when the foreground polarization is atypical. How sensitive the estimates of intrinsic polarization are with respect to the choice of ISP is illustrated by Leonard et al. (2000, see their Figure 10).

SNe 2008fp and 2014J were not as highly polarized as SN 2006X but showed a similar continuum polarization spectrum. Patat et al. (2015) combined the spectropolarimetric data of these three events with the multicolor polarimetry of SN 1986G, and performed a comparative analysis to try to understand the properties of extragalactic dust in the foreground of heavily reddened SNe Ia. They fitted their polarization spectrum with a Serkowski law and compared their K "constant" and $\lambda_{\rm max}$ with those of Galactic stars. They found that the K, $\lambda_{\rm max}$ pairs display an atypical interstellar behavior, and connected the small $\lambda_{\rm max}$ values with the presence of smaller than normal dust grains. Although the existence of CSM could not be excluded for these events, Patat et al. (2015) concluded that the dust responsible for the bulk of the polarization is interstellar. The reason why the highly extincted SNe show a polarization spectrum very different from that of extincted stars in the Galaxy was left open.

Hoang (2015) tried to answer whether pure ISM or combined CSM plus ISM models are a better fit to the observations of these SNe. He used a theoretical model of the dust grains with the size distribution and alignment as parameters. He confirmed that the low R_V values are a consequence of an enlarged proportion of small dust grains, and found that SNe 2006X and 1986G are better matched by pure foreground ISM while 2014J should carry a CSM-like component. His results are not completely conclusive in the case of SN 2008fp.

In this work, we combine the previously mentioned spectropolarimetric observations of SN 2006X, SN 2008fp, and SN 2014J with those of another 16 SNe observed with the VLT close to maximum light and at least one later epoch, to study the continuum polarization of suspected foreground origin in SNe with both large and small reddening. The high S/N ratio required to measure polarization allowed us to obtain high-quality low-resolution intensity spectra and made it possible to detect unresolved narrow lines of interstellar origin in some of them. We present the polarimetric spectra of these 19 SNe and show that 12 of them display unresolved Na I D absorption lines at wavelengths consistent with the redshift of their hosts. We do a closer analysis of the continuum polarization of these 12 SNe together with the multicolor broadband polarimetry of SN 1986G.

In Section 2 we briefly introduce the observations, which will be described individually in future works, as well as additional data that are relevant to this paper. In Section 3 we present our results on the polarization spectrum, reddening, and foreground absorption lines; in Section 4 we discuss them; and in Section 5 we summarize and present our conclusions.

2. Observations and Ancillary Data

We introduce here the polarimetric spectra of the 19 SNe Ia. Eighteen of them were observed with the VLT at ESO's Paranal Observatory and the remainder, SN 2014J, with the 2.2 m Telescope at Calar Alto Observatory.

SN 2014J was observed with the Calar Alto Faint Object Spectrograph.[9] A preliminary analysis of these data was done by Patat et al. (2014) and presented as well in Patat et al.

[9] http://w3.caha.es/CAHA/Instruments/CAFOS/

Table 1
Spectropolarimetry of the Na Sample, Hosts, Observed Equivalent Widths, and Polarization

SN	Date UT	Exposure (s)	Median Airmass	Host	Galaxy Type	Phase[a]	W_λ Na I[b] (Å)	W_λ Ca II[c] (Å)	P_{mean} %	Na Shift[d]
06X	2006 Feb 18.37	4 × 480	1.56	NGC4321	Sbc	−1	1.30(12)	0.97(31)	6.81(18)	B*
14J	2014 Jan 28.12	4 × 1200	1.27	M82	I0	−5	5.40(20)	2.01(31)	4.26(02)	⋯
08fp	2008 Sep 16.35	4 × 500	1.54	ESO428-G14	SAB0$\hat{0}$(r)pec	−3	2.15(07)	0.79(11)	1.93(06)	B*
07le	2007 Oct 21.23	4 × 300	1.56	NGC7721	SA(s)c	−4	1.42(08)	0.58(04)	1.71(08)	B*
10ev	2010 Jul 06.99	4 × 360	1.56	NGC3244	SA(rs)cd	−1	0.56(10)	0.32(17)	1.67(65)	S
02bo	2002 Mar 22.06	4 × 600	1.55	NGC3190	SA	−1	2.03(20)	0.72(07)	0.68(24)	⋯
07fb	2007 Jul 10.37	4 × 600	1.17	UGC12859	Sbc	−2	0.70(08)	0.55(20)	0.68(23)	B
03W	2003 Feb 03.24	4 × 1200	1.37	UGC05234	Sc	−6	0.63(03)	0.32(16)	0.56(32)	⋯
07af	2007 Mar 16.34	4 × 900	1.15	NGC5584	Scd	+1	0.41(10)	0.17(06)	0.44(40)	R
02fk	2002 Oct 01.30	4 × 720	1.02	NGC1309	SA(s)bc	0	0.04(01)	0.46(06)	0.33(16)	⋯
11ae	2011 Mar 04.19	4 × 500	1.06	UGCA254	SAB(s)cd	+2	0.20(08)	0.24(13)	0.21(09)	⋯
05hk	2005 Nov 09.14	4 × 900	1.26	UGC00272	SAB(s)d	−2	0.30(02)	⋯	0.13(37)	⋯

Notes.
[a] Phase (days with respect to *B* maximum light).
[b] Na I D equivalent width (Å).
[c] Ca II H and K equivalent width (Å).
[d] Shift of the Na D lines with respect to a principal Na D line component, measured in high-resolution spectra from Sternberg et al. (2011). B, R, and S denote blueshifted, redshifted, or single foreground Na I D lines, respectively. The symbol * denotes the reported time variability in some of the Na I D lines.

(2015). A full description of this observation will be given elsewhere.

The VLT observations were performed with two different spectrographs. Before 2008 April we used the FOcal Reducer and low dispersion Spectrograph, FORS1, at the UT2 Kueyen 8.2 m Telescope (Appenzeller et al. 1998), and after that date, we used FORS2, which inherited the polarimeter on FORS1 and was mounted at the UT1 Antu 8.2 m Telescope. All the observations were performed employing the same four half-wave plate angles (0°, 22.°5, 45°, and 67.°5), a 1.1 arcsec slit, and the low-resolution (112 Å mm^{-1}) grism G300V without an order separation filter attached, with the exception of SN 2006X and 2008fp for which we used the GG435 filter. A standard reduction procedure was followed (bias subtraction, flat fielding, and wavelength calibration) with the help of IRAF,[10] and sensitivity curves were computed for each supernova from flux standards observed at the same epoch at a position angle of the retarder plate of 0°. Flux calibration and Stokes parameters calculations were performed employing our own IDL routines, following the procedure described by Patat & Romaniello (2006) and the ESO FORS manual.[11] The resolution of the spectra, measured from the width of sky emission lines at ∼5900 Å, is 13.4 Å.

At least one subsequent observation, from ∼7 to ∼49 days after maximum light, was obtained for all of the SNe in Table 1. These later observations and a more comprehensive study of those introduced here will be provided in forthcoming publications.

We found that 12 of the 19 SNe in our sample displayed unresolved Na I D lines at velocities consistent with those of the parent galaxies. This subset of SNe is called the "sodium sample" in what follows. Some details of the observations, the SNe, and the parent galaxies, are presented in Table 1, including the equivalent width (EW) of the narrow, unresolved, Na I D lines. These were calculated using the SPLOT task in IRAF. The seven SNe for which we did not find foreground Na I D lines at the redshift of the host will be called the "non-sodium sample" in what follows. We found that 11 out of 12 SNe in our sodium sample displayed narrow interstellar Ca II H and K lines as well.[12] We measure the EW of these lines using the script described in Förster et al. (2012) and the results are also reported in Table 1.

Multicolor photometry is available for 11 of the 12 SNe in the sodium sample. Phillips et al. (2013) studied a sample of 32 SNe Ia with multiband photometry, in some cases extending to the infrared, and high-resolution spectroscopy of the foreground Na I D and K I λλ7655, 7699 lines. They provide estimates of color excess and R_V, and hence A_V, for 6 of the 12. Burns et al. (2014) present in detail the calculation of these parameters. Six of our events, SN 2002fk, SN 2003W, SN 2002bo, SN 2014J, SN 2005hk, and SN 2011ae, were not included in Phillips et al. (2013). Upon our request, Chris Burns has kindly calculated the $E(B-V)$, R_V, and A_V values and/or upper limits for the first two (SN 2002fk and SN 2003W). For the next two, SN 2002bo and SN 2014J, we rely on the values provided by Amanullah et al. (2014) and Krisciunas et al. (2004), and for SN 2005hk we follow Phillips et al. (2007). For SN 2011ae there were no public photometric data. We estimated its color at maximum light from our first spectrum taken two days after maximum light. The spectrum was corrected for the redshift of the parent galaxy and reddening in our Galaxy (Schlegel et al. 1998). We then computed a synthetic color by numerical integration through the *B* and *V* passbands given by Landolt (1992). The color uncertainty was obtained by integrating the spectrum flux with its reported observational error (see Table 2). For this SN we were unable to find extinction measurements.

[10] IRAF is distributed by the National Optical Astronomy Observatories,which are operated by the Association of Universities for Research in Astronomy, Inc., under cooperative agreement with the National Science Foundation (http://iraf.noao.edu).
[11] For details of the instrument check the FORS Manual at http://www.eso.org/sci/facilities/paranal/instruments/fors/doc/.
[12] When our spectra did not reach the wavelength range of the calcium lines, we used those of the public SN database of the Center for Astrophysics (Blondin et al. 2012) and the Carnegie Supernova Project (CSP) (Folatelli et al. 2013).

Table 2
Color, Color Excess, Extinction, and R_V[a]

SN	$(B-V)_{B\,\max}$	$E(B-V)$	A_V	R_V	$A_{V,MW}$	References[b]
06X	1.26(05)	1.36(03)	1.88(0.11)	1.31(0.09)	0.07	phi13, bur14, hic09
14J	1.25(06)	1.37(03)	1.85(0.11)	1.40(0.10)	0.44	ama14, mar15
08fp	0.67(01)	0.58(02)	0.71(0.09)	1.20(0.21)	0.54	phi13, bur14
07le	0.28(04)	0.39(02)	0.54(0.08)	1.46(0.28)	0.09	phi13, bur14, gan10
10ev	0.36(05)	0.32(03)	0.50(0.18)	1.54(0.58)	0.28	gut11, phi13, burnspc
02bo	0.37(07)	0.53(03)	0.62(0.10)	1.22(0,26)	0.07	phi13, kris04, ben04, hic09, gan10
07fb	−0.06(01)	$\lesssim$0.03	$\lesssim$0.09	2.17(0.57)	0.15	phi13, burnspc
03W	0.16(01)	0.29(04)	0.30(19)	1.0(0.70)	0.13	burnspc, hic09
07af	0.08(05)	0.15(02)	0.31(06)	2.11(0.51)	0.10	phi13, bur14
02fk	−0.12(06)	0.02(01)	0.03(02)	1.73(1.02)	0.11	burnspc, hic09
11ae	0.03(02)	…	…	…	0.16	…
05hk	−0.03(04)	0.07(02)	0.22(0.06)	3.1	0.06	mau10, phi07, cho06, hic09, sah08

Notes.
[a] Values corrected for extinction in the Milky Way (Schlafly & Finkbeiner 2011).
[b] ama14—Amanullah et al. (2014), mar15—Marion et al. (2015), bur14—Burns et al. (2014), burnspc—C. Burns personal communication, phi13—Phillips et al. (2013), gut11—Gutiérrez et al. (2011), gan10—Ganeshalingam et al. (2010), mau10—Maund et al. (2010a), hic09—Hicken et al. (2009), sah08—Sahu et al. (2008), phi07—Phillips et al. (2007), cho06—Chornock et al. (2006), kri04—Krisciunas et al. (2004), ben04—Benetti et al. (2004).

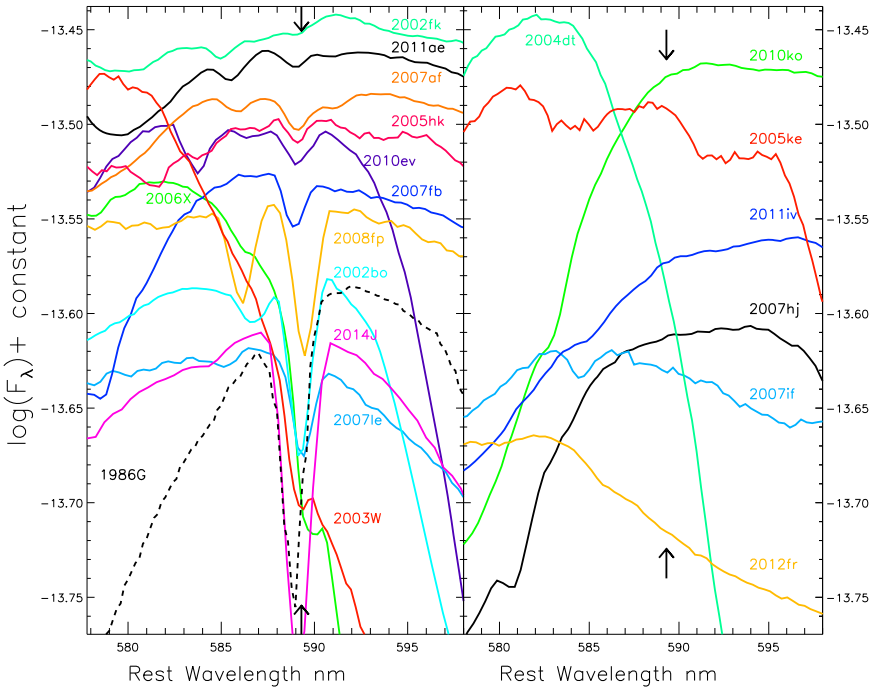

Figure 1. Rest-frame low-resolution intensity spectra of the 19 SNe in our sample. The left panel shows the sodium sample, and the right panel the non-sodium one. The position of the Na I D lines at the redshift of the SN hosts is indicated by arrows.

Finally, we incorporated SN 1986G, which exploded in Centaurus A and was intensively observed. A wealth of data is publicly available, including multicolor broadband polarimetry. The data relevant to this paper are presented in the Appendix.

3. Results and Analysis

The intensity spectra of the 19 SNe, in a rest-frame wavelength range bracketing the Na I D lines, are displayed in Figure 1. The left panel shows the sodium sample and the right one the non-sodium sample. The logarithmic vertical scale of both panels is the same. The left panel displays a large diversity of EWs, from very small as in the case of SN 2003W, up to very large as in the cases of SN 2002bo or SN 2014J. Some SNe display, in addition, Na I D lines produced by interstellar matter in our Milky Way. In the case of SN 2014J, the Na I D lines of the Milky Way and those of the parent galaxy appear blended at the resolution of our observations. High-resolution spectra, however, reveal that the Galactic component is negligible in comparison with that of the host (A. Sternberg et al. 2014, in preparation; Patat et al. 2015).

The right panel reveals that SNe in the non-sodium sample show no trace of absorption at the expected rest-frame wavelength of the Na I D lines. To quantify the absence with upper limits, we fitted Gaussian profiles of the spectra resolution at the expected wavelengths of the lines. We found that the EW of the Na I D line is smaller than 0.03 Å for SN 2007if and smaller than 0.01 Å for the other six SNe in the non-sodium sample. Some of the SNe in the non-sodium

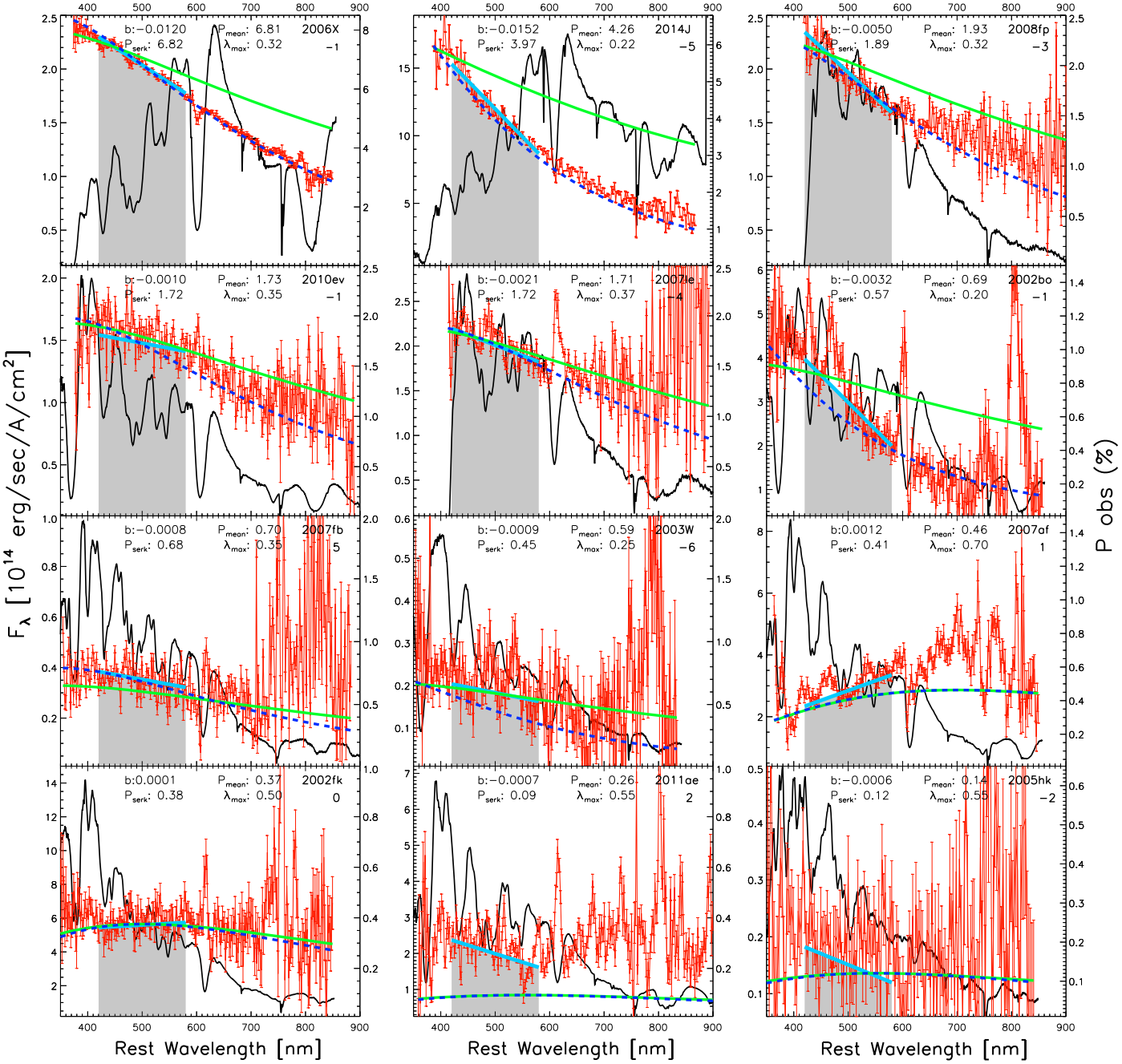

Figure 2. Polarization and intensity spectra of the SNe in the sodium sample (see Table 1). The left vertical axes give monochromatic flux and the right axes percent polarization. Note that the vertical scales are different in different panels. The polarization spectrum is represented by the red solid line and the intensity spectrum by the black solid line. The blue dashed line is the original Serkowski law (our Equation (1), Serkowski et al. 1975). The green dotted–dashed line is Serkowski's law with parameter K given by Equation (2) (Whittet et al. 1992). The gray-shaded area marks the wavelength range 420–580 nm, used to fit a straight line to the observed polarization spectrum. The fit is plotted with the cyan line. The parameters of the fit, slope b and mean percent polarization $P_{\rm mean}$, are given at the top of each panel. From top left to bottom right, the panels show a decreasing $P_{\rm mean}$ or, equivalently, decreasing shaded area.

sample display Na I D lines in the interstellar matter in the Milky Way. Since, in the sodium sample, host galaxy Na I D lines are typically at least as strong as the galactic ones, this suggests that the non-detections are real.

Figures 2 and 3 exhibit the polarization and flux spectra of the SNe in the sodium and non-sodium samples, respectively. The observations in both figures illustrate the variety of spectropolarimetric properties of SNe Ia near maximum light. Some of them exhibit strong line polarization while others display a relatively featureless polarization spectrum. The analysis of the line polarization is beyond the scope of the present work, where we study the continuum polarization spectra.

We decided to constrain the analysis of the polarization spectra to the wavelength region between 420 and 580 nm. We did so first because it is a region with good signal-to-noise ratio in our spectra, second because the continuum polarization of our sodium sample tends to be higher in this range, and finally, because most of the imaging polarimetry in our Galaxy and neighbors has been observed in the V band passband, which makes this a convenient interval to facilitate comparisons. This wavelength region of interest has been shaded in gray in

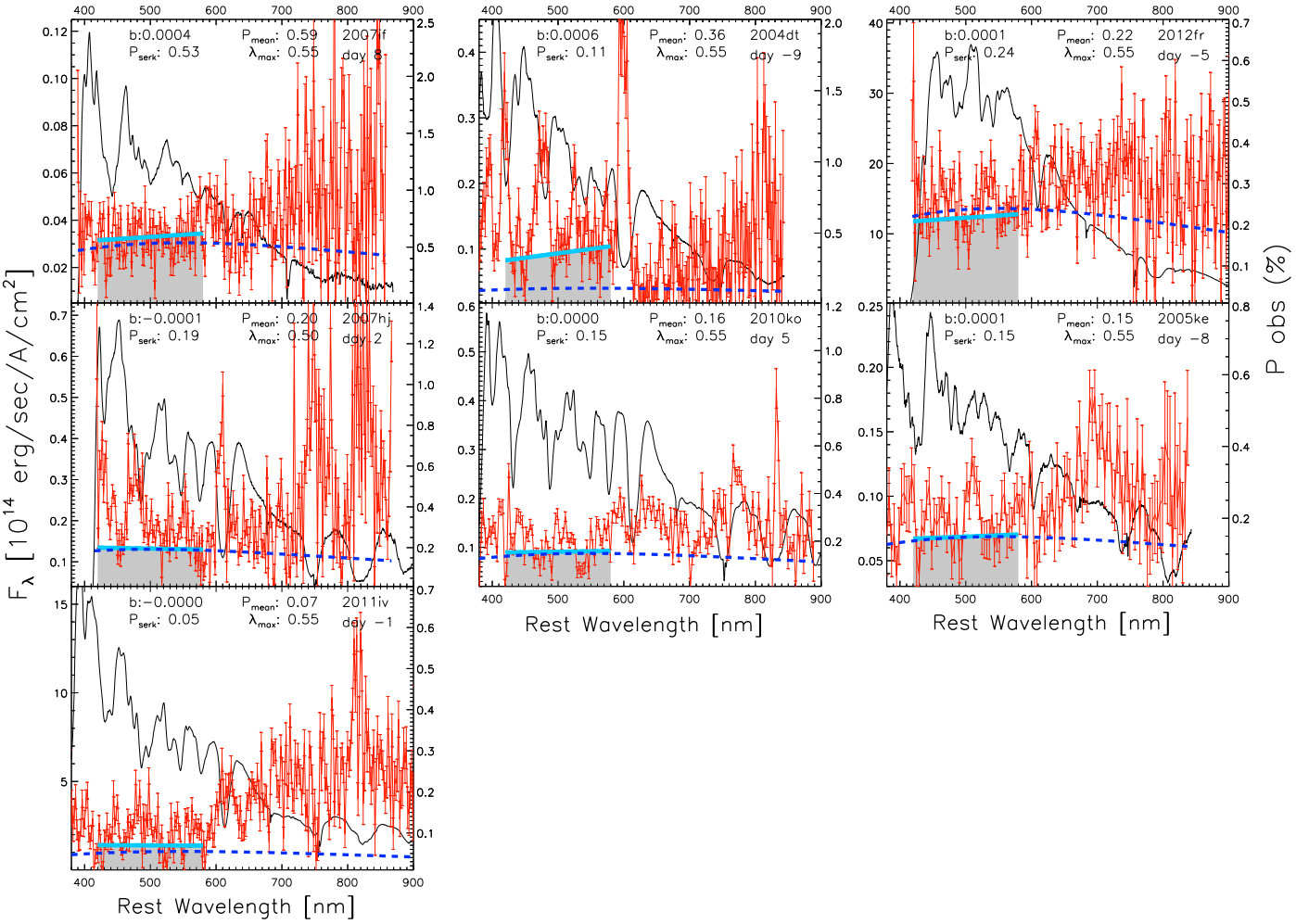

Figure 3. Same as Figure 2 for the polarization and intensity spectra of the seven SNe that did not show narrow Na I D lines at the velocity of their hosts in our low-resolution spectra.

Figures 2 and 3. The area of the shaded regions, which is proportional to the average polarization in the range, was used to organize the SNe in a sequence of decreasing average polarization from the upper-left to the lower-right panels.

Comparing the gray areas of the continuum polarization spectra of SNe in Figure 2 with those of Figure 3 reveals that most of the SNe in the sodium sample show continuum polarization with a negative slope, and that this slope decreases together with the area of the shaded region. Also, for most SNe in the sodium sample, the shape of the polarization spectrum is approximately linear in the selected range. This is shown by a fitted cyan line (to be defined below). These characteristics seem to be independent of the presence of line polarization, which for some SNe is obvious (e.g., SN 2007le and 2002bo in the sodium sample, and 2004dt and 2007hj in the non-sodium one) while for some others it is not that clear (e.g., SN 2008fp in the sodium sample and 2007if in the non-sodium one). Finally, there is some continuity between Figures 2 and 3. The continuum polarization spectra of SNe with small average polarization (i.e., those in the lower panels of Figure 2) tend to be more similar to the continuum polarization spectra in Figure 3, while those of SNe with sizable mean polarization (i.e., those in the upper panels of Figure 2) are quite different.

All SNe in the sodium sample have later-time spectro-polarimetric observations, extending from about a week up to several weeks after maximum light (seven in the case of SN 2006X). These later observations are partially shown in Figure 4, where the observed continuum polarization of each SN is computed as the average polarization in the region between 400 and 600 nm, with 3σ deviant values rejected. The figure shows that, irrespective of the evolution of the SN light curves and flux spectrum, the polarization varies by less than 0.05% on average. The exception is SN 2011ae, which shows a variation of 0.08% in the continuum polarization between our two epochs. We take this variation as evidence of intrinsic continuum polarization and, since the expectations are that this polarization will decrease as the SN ages (Wang & Wheeler 2008), we estimated the ISP using the latest observation. This is why both the Serkowski and the Serkowski–Whittet profiles in Figure 2 fall below the continuum polarization of the first epoch.

Another important observable of the polarimetric signal is the direction of the polarization angle. In the wavelength region between 420 and 580 nm, the direction of polarization is wavelength independent. There is no rotation of the polarization angle.

Also, the polarization pseudo-vectors of almost the entire sodium sample are aligned with major features of the hosts projected at the position of the SNe, like the spiral arms or the disk of the host galaxy. This is particularly relevant in the case

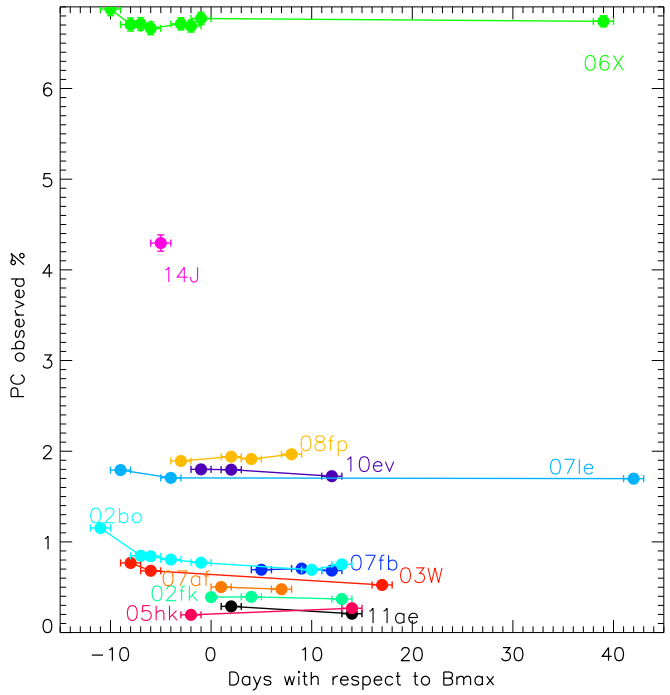

Figure 4. Evolution in time of the observed continuum polarization for the sodium sample (see the text for a definition of continuum polarization).

of SN 2008fp, which shows a prominent Na I D line caused by matter in the Milky Way. As noted before by Cox & Patat (2014), a contribution to the ISP from our galaxy is expected, but the orientation of the observed polarization suggests that it is not very significant. Orientation with host structures is not very evident in the non-sodium sample where the polarization angles seem to be randomly oriented with respect to the major features of the hosts. This is due to the low polarization values in that sample, which are associated with large error bars (see Figures 5 and 6), and also to the relatively larger impact of Galactic polarization components.

Indications are, then, that the observed continuum polarization of the SNe in the sodium sample is ISP, albeit of a peculiar character, produced predominantly by foreground matter in the host galaxy. Even though the ISP of some SNe might have a Galactic component, we fit a unique ISP and assume it belongs mainly to the host galaxy. The assumption is supported by both the alignment of the polarization angle with the local structure of the host (see Figure 5) and the Na I absorption lines of extragalactic origin, which are always dominant compared to the Galactic ones (see Figure 1), and is further justified in Section 4.

Accordingly, we attempted to fit these polarization spectra with a single Serkowski et al. (1975) ISP law:

$$P(\lambda) = P_{\max} \exp\left(-K \ln^2 \frac{\lambda_{\max}}{\lambda}\right), \quad (1)$$

where $P_{\max}$, the maximum polarization, and $\lambda_{\max}$, the wavelength at which the maximum polarization occurs, are free parameters, and K is a constant. We take $K = 1.15$ from Serkowski et al. (1975). These curves are shown by a dashed blue line in Figure 2. The green dotted–dashed lines correspond to the modification of the Serkowski profile proposed by Whittet et al. (1992), in which the constant K is replaced by

$$K = 0.01 \pm 0.05 + (1.66 \pm 0.09)\,\lambda_{\max}, \quad (2)$$

with $\lambda_{\max}$ in microns.

Fitting either of Equations (1) or (2) to our observations requires values of $\lambda_{\max}$ in the range 0.20–0.40 μm for 8 of the 12 SNe in the sodium sample. This wavelength range is unusually short in comparison with the typical values found for the ISP of the Milky Way ($\lambda_{\max} \sim 0.55$ μm). Three of the remaining, SNe 2011ae, 2002fk, and 2005hk, have Milky Way-like values of the peak wavelength, and SN 2007af demands a longer wavelength ($\lambda_{\max} \simeq 0.75$ μm).

The $\lambda_{\max}$ parameters of the SNe in the sodium sample make them an atypical group when compared with the standards of the Milky Way. This is better illustrated by the histograms shown in Figure 7 where we compare the distribution of $\lambda_{\max}$ for the sodium and non-sodium samples with that of stars in the Galaxy (from Serkowski et al. 1975). Finally, Figure 2 shows that the Serkowski–Whittet polarization spectrum gives a poor fit to the observed polarization, especially in those objects that have higher polarization in the blue continuum. This had been quantitatively shown by Patat et al. (2015) for the highly polarized SNe 2006X, 2008fp, and 2014J (see their Figure 2).

It is seen in Figure 2 that for the small values of $\lambda_{\max}$ found, the original Serkowski law approaches a straight line, especially in the blue part of the spectrum. We have found it most useful to build upon this similarity and describe the observed polarization by modeling it with a straight line fitted to the wavelength range 420–580 nm (the region shaded in gray in Figures 2 and 3). Line blanketing in this range is strong and even if the scattering photosphere was asymmetric, and its emission was intrinsically polarized, the blanketing by different lines in different regions of the overlying expanding atmosphere, mainly by iron lines, will provide for almost complete depolarization (Wang et al. 1997; Howell et al. 2001). Hence, the observed continuum polarization in this region can be reasonably attributed to foreground sources. Finally, characterizing the foreground polarization in this region facilitates the comparison with observations made with imaging polarimeters, typically performed at B and/or V bands.

Irrespective of the previous considerations on the continuum polarization, some of our SNe do show line polarization in the wavelength range between 420 and 580 nm. This is particularly clear in SNe with smaller overall polarization, like SNe 2004dt and 2007hj in the non-sodium sample. The line polarization is typically associated with the absorption troughs of Si III 4560, Si II 5051, the S II multiplets between 5468 and 5654 Å and, in some cases, the Mg II line at 4481 Å. To reduce the influence of this line polarization in our estimates of the continuum polarization, we performed a two-step iteration of the linear fit, excluding in the second step the points that were 2σ above the fit of the first step.

The linear fits of polarization in our chosen wavelength range can be written as

$$P_{\rm cont}(\lambda) = a + b\lambda, \quad (3)$$

and are shown in Figures 2 and 3 by a cyan line. We choose to characterize the observations by the slope b of the fitted straight lines and the value of the mean continuum polarization $P_{\rm mean}$,

$$P_{\rm mean} = P_{\rm cont}(500\ {\rm nm}), \quad (4)$$

since 500 nm is the average wavelength of the selected region.

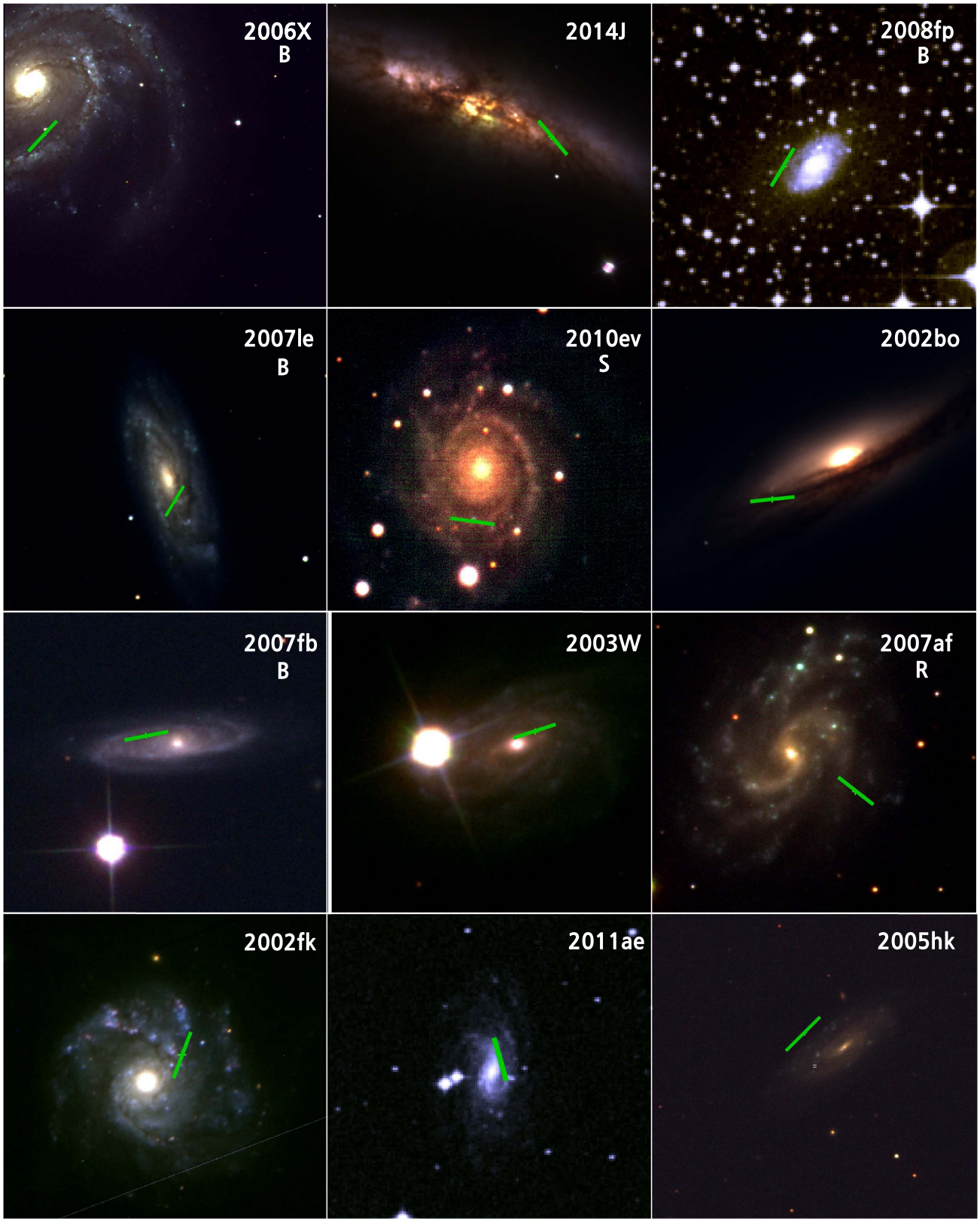

Figure 5. Orientation of the polarization angle for the 12 SNe in the sodium sample. The bars are centered at the position of the SNe. North is up and east is to the left. Labels B, S, and R correspond to Sternberg's classification of the sodium line shift.

We understand the observed continuum polarization to be the result of anisotropic extinction by aligned dust grains. If so, the slope b in the selected wavelength range depends on the physical processes that polarize the light both at the microscopic and macroscopic scales. The intrinsic properties of the ensemble of dust grains, like size and asphericity, determine the relative polarizing efficiencies at different wavelengths, and, in particular, in the [420, 580] nm

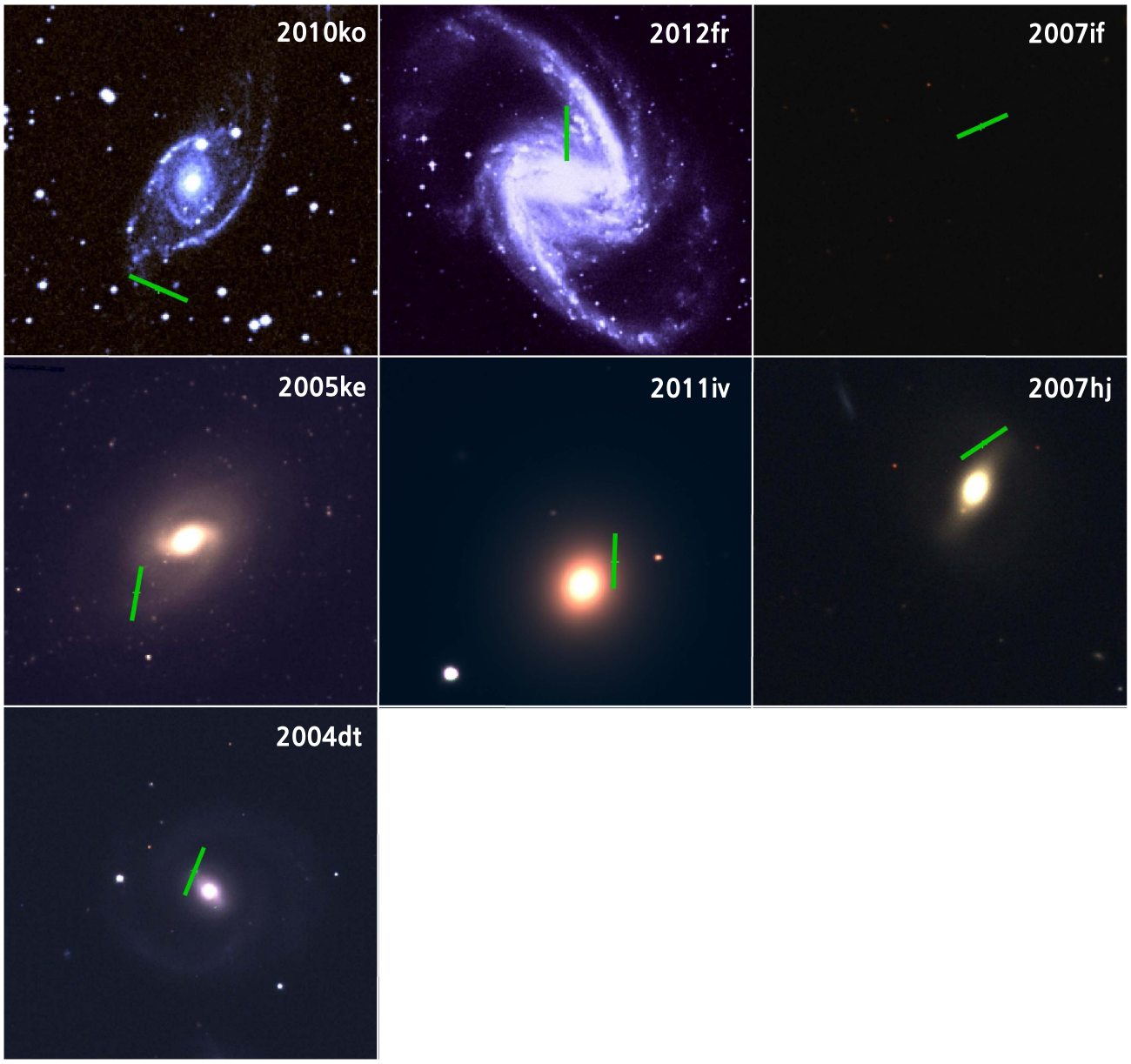

Figure 6. Same as Figure 5 for the seven SNe in the non-sodium sample.

wavelength range. If λ_{max} is to the blue of 420 nm, then $b < 0$, and the closer λ_{max} is to ~500 nm, the shallower the slope b will be. On the other hand, for λ_{max} not within the [420, 580] nm wavelength range, a larger efficiency of grain alignment, a more ordered magnetic field, or larger amounts of dust imply a larger P_{max} and, hence, a steeper slope b (more negative if $\lambda_{max} \lesssim 420$ nm and more positive if $\lambda_{max} \gtrsim 580$ nm). For λ_{max} close to, or within, the [420, 580] nm wavelength range, an increase of P_{max} will not result in an appreciable change of the slope b.

The mean continuum polarization, P_{mean}, is a measure of the average polarization over a broad wavelength range, akin to a broad passband filter measurement. For small values of polarization, it should be an additive quantity in the Stokes parameters' space, summing over the contributions of different polarizing regions. If the light goes through different dusty regions with magnetic fields well-organized over large distance scales, the size of P_{mean} will be a combined measure of dust column density and alignment efficiency. If the dust properties of different regions are similar and result in similar values of λ_{max}, the combined polarization will have a larger P_{max} and steeper slope for wavelengths sufficiently smaller, or sufficiently larger, than λ_{max}. If the dust properties of different regions are different and result in different values of λ_{max}, the combined polarization will have a larger P_{max} as well. But there will be a broader maximum in the polarization spectrum and the slope at wavelengths bluer or redder than the maximum will be shallower. Finally, the combined contribution of regions with randomly oriented magnetic fields should statistically result in no net polarization, although the combination of a few regions with different dust properties could result in rotation of the polarization angle with wavelength.

We found that the b and P_{mean} parameters are well correlated (see Figure 8). The correlation coefficient of the linear

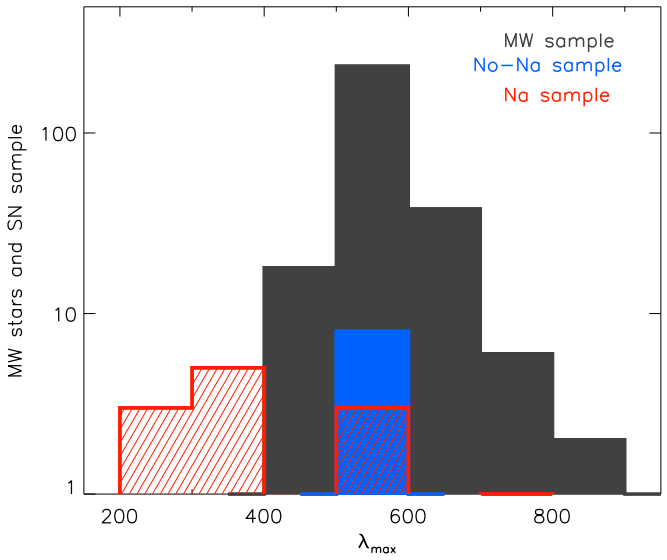

Figure 7. Histogram of λ_{max} for SNe in the sodium sample (red shaded area), the non-sodium sample (blue filled area), and stars in the Galaxy (shaded in dark gray).

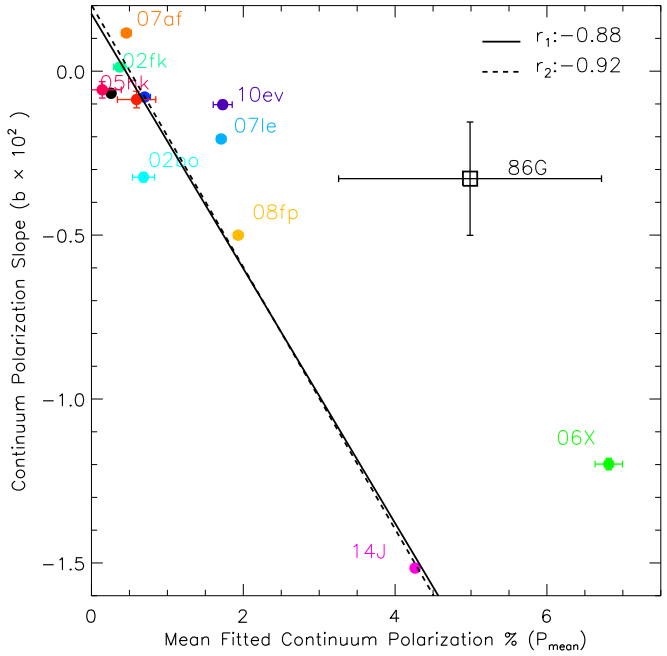

Figure 8. Correlation between the parameters b and P_{mean} that describe the observed continuum polarization (see the text and Figure 2). The solid line shows the linear fit to all points (correlation coefficient r_1) and the dashed line the linear fit when SN 2006X is excluded (correlation coefficient r_2).

regression is −0.88 when all the objects with spectropolarimetric observations are used.[13] The regression is shown with a solid line and indicates a tight fit. Both SNe 1986G and 2006X appear to be outliers, showing a polarization larger than expected from the slope of the blue continuum. If SN 2006X is removed from the sample (we stress that SN 1986G is displayed in the figures, but not included in the fits), the correlation coefficient becomes −0.90 (shown by a dashed line in the figure). Either with or without SN 2006X, the probability of obtaining these correlation coefficients by chance if b and

[13] SN 1986G is excluded from all computations of correlation coefficients, because it was observed with a very different technique.

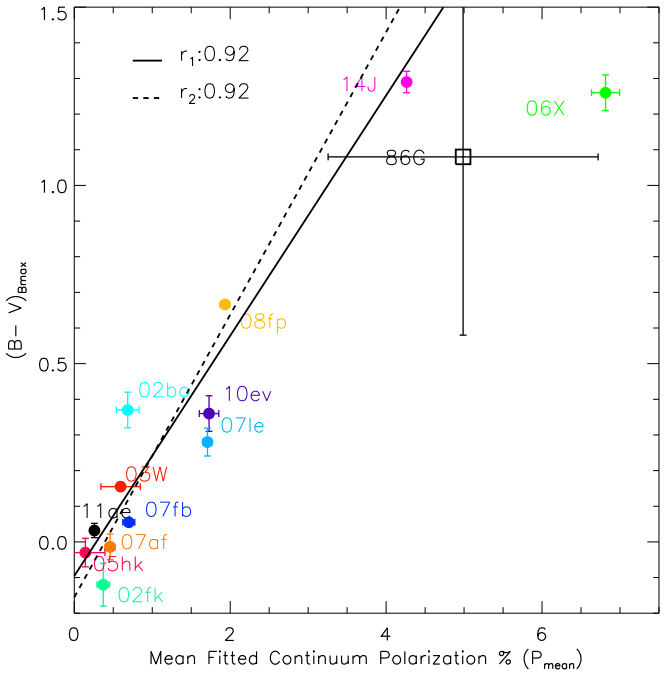

Figure 9. Correlation between the observed color at maximum light and the continuum polarization. As in the previous figure, the solid line shows the fit to the entire sample and the dashed line excludes SN 2006X. The correlation coefficients are r_1 and r_2, respectively.

P_{mean} were not correlated is smaller than one percent. The implied linear relation allows us to use either b or P_{mean} as a single parameter to describe the observed continuum polarization. We choose to use P_{mean} in what follows because it is easier to interpret.

Having P_{mean} as the single parameter to describe the amount of observed polarization, we can look for correlations between it and other observables in Tables 1 and 2. We have found that P_{mean} correlates with the observed color at maximum light (see Figure 9). The correlation coefficient for a linear regression when all of the SNe are used in the fit is 0.90, and when SN 2006X is excluded it is 0.95. We have also found that P_{mean} correlates very well with the extinction and color excess measured by Phillips et al. (2013) and Burns et al. (2014) (see Figures 10 and 11). The correlation coefficients for a linear regression between P_{mean} and extinction when all of the SNe are fitted is 0.89, and increases to 0.91 when SN 2006X is excluded. For the linear fit between P_{mean} and $E(B-V)$ the correlation coefficients result in 0.82 and 0.85 for the cases including and excluding SN 2006X, respectively. The probability of obtaining these correlation coefficients by chance if the observables were not correlated is, in all cases, smaller than one percent.

The correlation between P_{mean} and the EWs of the Na I D and Ca II H and K lines of the hosts is poorer (see top panels in Figure 12). It is more of a triangular region where at low polarization values, little or no Na I D lines are found, but at higher polarization values a wide range Na EW is found. For the Na I D lines, linear regressions provide correlation coefficients of 0.24 for the complete sample and 0.56 when SN 2006X is excluded, while for the Ca II H and K lines the results are 0.37 and 0.57, respectively. The correlation coefficients when SN 2006X is included are not very significant. The probability of obtaining them by chance if the EWs of the lines and polarization were not correlated are 41% and 22% for the Na I D and Ca II H and K lines,

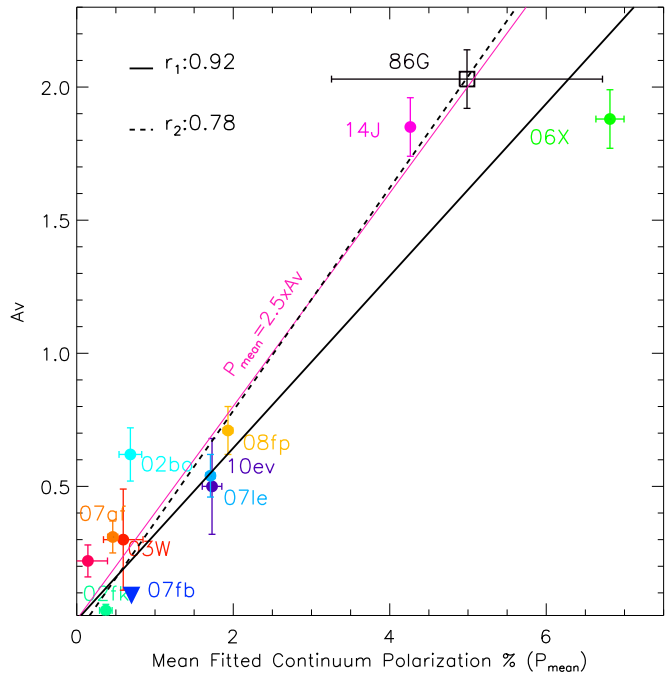

Figure 10. Correlation between the extinction in the visual band and $P_{\rm mean}$. The solid line shows the linear fit to all points and the dashed line the linear fit when SN 2006X is excluded (correlation coefficients r_1 and r_2, respectively). Downward pointing triangles are upper limits to A_V.

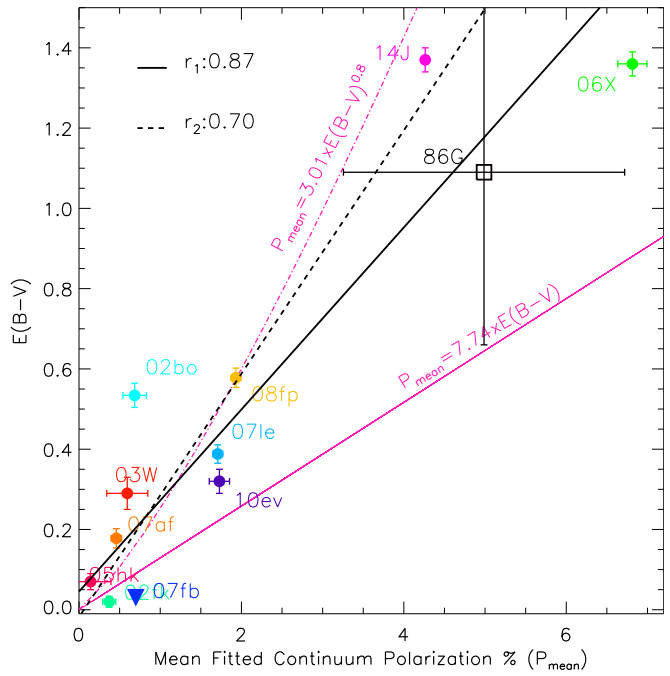

Figure 11. Correlation between the color excess $E(B-V)$ and $P_{\rm mean}$. As in the previous figures, the black solid line shows the linear fit computed for the entire sample and the black dashed line the linear fit when SN 2006X is excluded. The correlation coefficients are r_1 and r_2, respectively. The magenta solid line shows the upper limit of the polarization for a given color excess $E(B-V)$ found by Serkowski et al. (1975) for stars in the Galaxy. The magenta dotted–dashed line is the mean relation found by Fosalba et al. (2002), also for stars in the Galaxy, given by their Equation (3).

respectively. When SN 2006X is excluded they become marginally significant, with the probability of being obtained by chance of 6% and 7% for the Na I D and Ca II H and K lines, respectively. The overall shape of the figures suggests that there are upper and lower envelopes that limit the observed polarization given an EW of foreground lines of either Na I D or Ca II H and K. The correlation between the EWs of the Na I D and Ca II H and K lines for each SN is good, as expected for normal interstellar media (bottom panel in Figure 12).

The relation between R_V and the mean polarization appears to be more complex. This is presented in Figure 13 as the R_V estimates given in Table 2 plotted against $P_{\rm mean}$. SNe with low values of $P_{\rm mean}$ and small EWs of Na I D display a wide range of R_V values, although they tend to be smaller than the typical Galactic value. SNe with high polarization ($\gtrsim$1%) and large EWs of Na I D appear to scatter around a low constant value ($R_V \sim 1.5$). Taking the weighted mean of the 10 R_V in Table 2 that have a reported uncertainty, one obtains $R_V = 1.50 \pm 0.06$ for the sodium sample (shown by a red horizontal line in Figure 13). In Figure 13 we have included the R_V estimates given by the relation $R_V \simeq 5.5\lambda_{\rm max}$ (Serkowski et al. 1975). They are plotted with black stars and qualitatively follow the same trend as the photometric estimates: a scatter at low polarization and a convergence to $R_V \sim 1.5$ at larger polarization.

4. Discussion

We chose to study the properties of the sodium sample presented in Figure 2 because we noted that the steepness of the slope of the polarization with wavelength increased with the EW of the Na I D lines, and the highly polarized cases could not be described by a standard Milky Way ISP. The preponderance of the Na I D lines at the redshifts of the hosts and the orientation of the polarization pseudo-vectors indicate that most of the reddening and polarization in these SNe originate in their own galaxies. Also, fitting a Serkowski ISP law to 8 of these 12 SNe requires an average wavelength of maximum polarization $\lesssim$350 nm, a low and fairly unusual value by Milky Way standards. On the other hand, the observed continuum polarization of the SNe in the non-sodium sample could be reasonably well-fitted with a Serkowski-type ISP with wavelength of maximum polarization close to 550 nm, the typical value for the Milky Way. This, together with the lack of Na I D lines at the redshifts of the hosts, suggests that most of the reddening and polarization in this group is produced in the Galaxy. The host foreground Na I D lines and the unusual ISP make these 12 SNe in the sodium sample special with respect to the other seven.

The emphasis in this work is on the relationship of the continuum polarization to dust properties, and it is fairly clear that for the most polarized objects, those on the top panels of Figure 2, dust polarization is the dominant one. The objects with smaller continuum polarization, however, will be more sensitive to putative intrinsic signals. This is compounded by the fact that the latest epoch of the seven SNe with the smallest continuum polarization in the sodium sample was obtained between eight and eighteen days after maximum light, that is, at times early enough to suspect that intrinsic components could be present (see Figure 4). The case of SN 2011ae was already noted in Section 3 and treated separately. Another SN worth mentioning is SN 2007af. This event is an outlier both in the wavelength of maximum polarization and the orientation of the polarization angle. Also, the continuum polarization rises toward the red up to ~700 nm. An increase in continuum polarization starting at ~6500 nm and growing toward longer

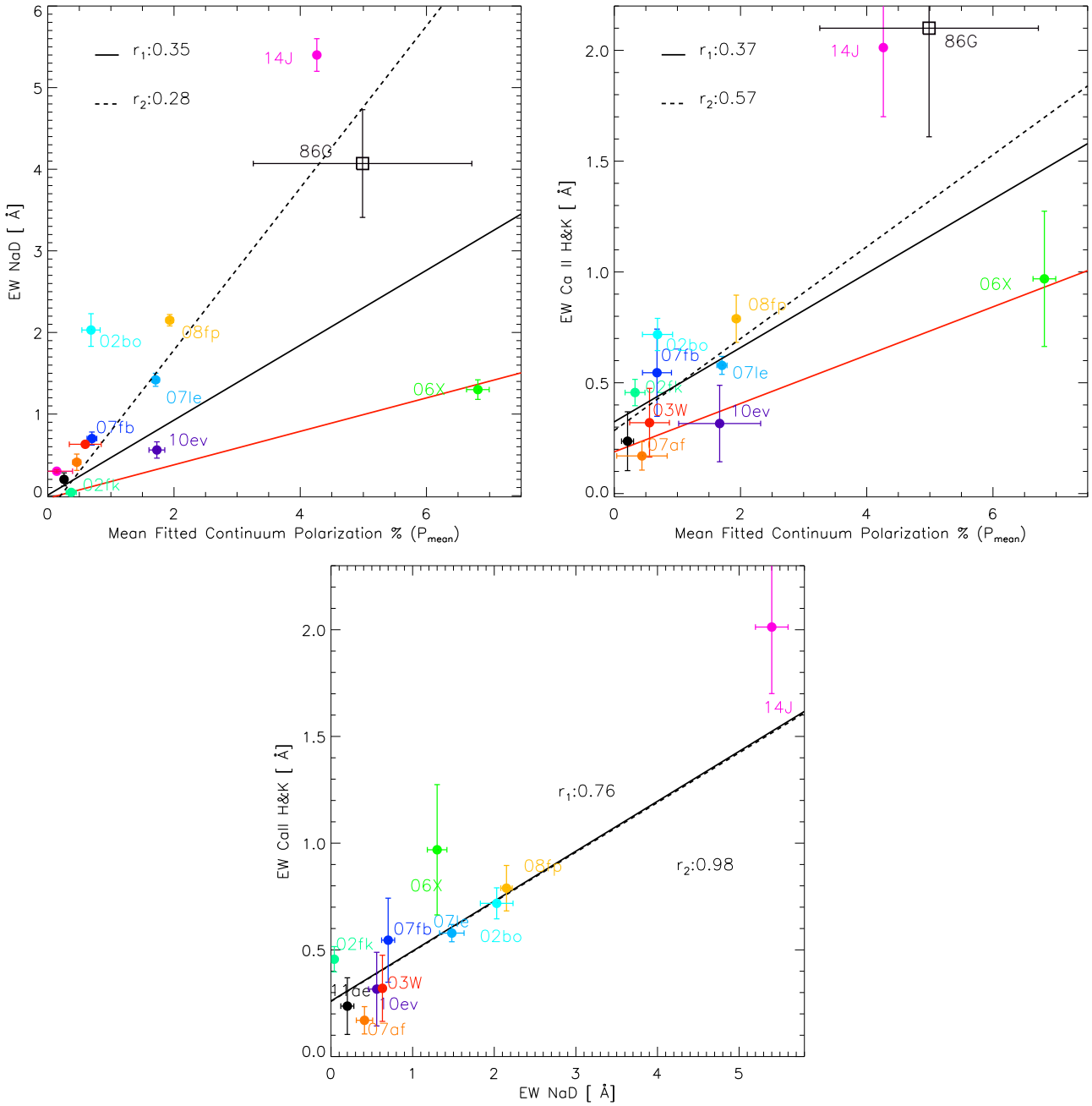

Figure 12. Correlation between the EW of the narrow lines of foreground origin and $P_{\rm mean}$. Na I D is shown in the top-left panel and Ca II H and K in the top-right panel. As in previous figures the black solid line shows the linear fit computed for the entire sample and the black dashed line shows the linear fit when SN 2006X is excluded. The solid red lines are approximate upper limits to the observed continuum polarization given the EW of the foreground absorption lines. The bottom panel shows the correlation between the EW of the Na I D and Ca II H and K lines for each SN.

wavelengths was observed in spectropolarimetric models by Wang et al. (1997), and was explained as the result of decreasing line blending toward longer wavelengths. This behavior was observed by Howell et al. (2001) in SN 1999by. The continuum polarization of SN 2007af, however, is different from that of SN 1999by in that it does not show the break in the slope expected on theoretical grounds but rises monotonically from the blue side of the spectrum. The peculiarity of SN 2007af may be due to an intrinsic signal or to aligned foreground dust with a size distribution biased toward larger grains. In general, contributions from intrinsic continuum polarization at a fraction of a percent level in some of our SNe cannot be ruled out. Nevertheless, from the standpoint of this work, they imply an increase in the scatter that is more noticeable at the low polarization levels in Figures 8–13. A more involved analysis of individual SNe will be done in forthcoming papers.

4.1. Polarization by Foreground Dust

As shown in Section 3, the continuum polarization of the SNe in the sodium sample can be reasonably well-matched by a Serkowski law using the original constant K and different values of $\lambda_{\rm max}$ that do not generally follow the Whittet relation (Equation (2)). Eight of them require $\lambda_{\rm max} \lesssim 0.36\,\mu$m, where two extreme cases, SN 2014J and 2002bo, were fitted with

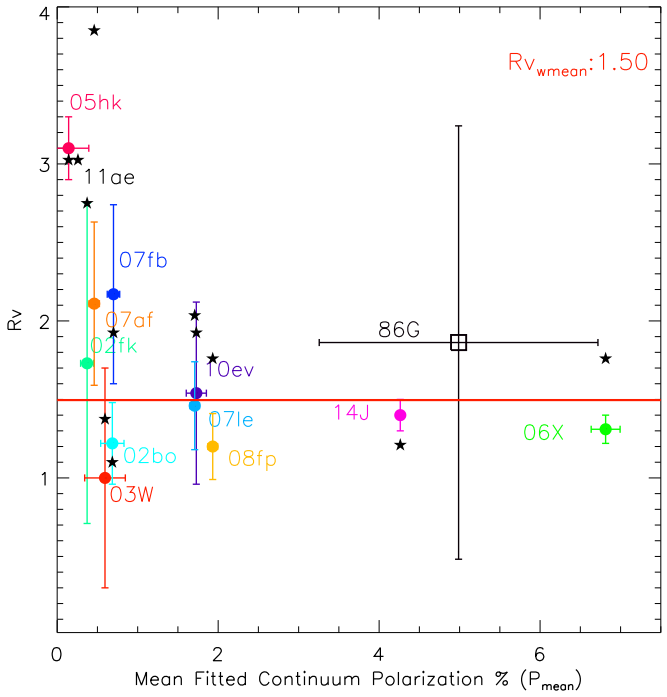

Figure 13. R_V values vs. the continuum foreground polarization parameter $P_{\rm mean}$. Black stars correspond to the R_V predicted by the relation $R_V = 5.5\,\lambda_{\rm max}$ found by Serkowski et al. (1975) for stars in the Galaxy. The red horizontal line is the weighted average of the 10 SNe that have a reported uncertainty ($R_V = 1.5 \pm 0.06$).

$\lambda_{\rm max} \sim 0.22\,\mu$m. On the other hand, SNe 2011ae, 2002fk, and 2007af require $\lambda_{\rm max} \sim 0.45$, 0.55, and 0.75 μm, respectively. Failures of the Whittet relation have been reported earlier by Hough et al. (1987) in their study of the broadband polarization of SN 1986G, which appeared behind the dust lane of Centaurus A, and by Patat et al. (2009), while Patat et al. (2015) studied in detail the mismatch for the cases of SNe 2006X, 2008fp, and 2014J. Non-compliance with the Whittet relation could be a general property of regions with short $\lambda_{\rm max}$.

An ISP model matched by a Serkowski law strongly suggests that the observed continuum polarization originates in selective extinction by anisotropic dust grains oriented by a large-scale magnetic field in the circumstellar/ISM of the parent galaxies. This conclusion is consistent with the observed polarization being constant in time, and with angles of polarization that tend to align with major large-scale features of the host galaxies projected at the SN position (see Figure 5).

The close correlation between the observed slope b and $P_{\rm mean}$ can be understood as the result of polarization by regions of aligned dust, organized by the same large-scale magnetic field, if $\lambda_{\rm max}$ is located to the blue of the [420, 580] nm wavelength range. In these conditions, $P_{\rm mean}$ will closely follow the behavior of Serkowski's $P_{\rm max}$ increasing together with the slope steepness as the optical depth of the aligned anisotropic dust grows. Particular configurations or arrays of dust clouds can affect both $P_{\rm mean}$ and b in different ways, as mentioned earlier for the possible relations between $P_{\rm max}$ and b. Let us consider, as an illustration, two dusty regions located at different distances from the SN. Assume that region 1 imprints a foreground polarization P_1, due to elongated dust grains of characteristic size λ_1, aligned with the local magnetic field. If the more distant region 2 is composed of dust with the same characteristic size, aligned by the same magnetic field, the total polarization $P_{\rm mean}$ will be increased ($P_{\rm mean} > P_1$), but the peak of polarization will remain at the same wavelength λ_1. However, if region 2 contains dust grains aligned by the same magnetic field, but with a different characteristic size $\lambda_2 > \lambda_1$, the total polarization $P_{\rm mean}$ still increases but the maximum polarization efficiency will be shifted to wavelengths longer than λ_1. If the light passes through several regions with different types of dust and different orientations of the organizing magnetic fields, the net effects will be depolarization and rotation of the polarization angle with wavelength.

The correlation between $P_{\rm mean}$ and b, and the lack of rotation of the polarization angles, suggest that most of the polarization is imprinted in a few dusty regions threaded by the same large-scale magnetic field. The polarizing dust in these regions must have similar properties, resulting in similar, typically small, values of $\lambda_{\rm max}$. Under these conditions, the polarization would be approximately described by a single Serkowski law (Patat et al. 2010) and the correlation arises naturally.

4.2. Polarization and Photometry

As expected for polarization produced by aligned dust on SNe Ia, whose intrinsic colors near maximum light fall within a narrow range, there is a connection between $P_{\rm mean}$ and color, color excess, and A_V (Figures 9–11). These connections are broadly similar to the mean relations between polarization and other photometric signals of dust found in the Galaxy. The tight correlation between SN color at maximum light and $P_{\rm mean}$ in Figure 9, especially when SN 2006X is removed from the fit, is expected. Normal SNe Ia have a fairly uniform blue color near maximum light so most of the observed spread in color ought to be due to extinction. Note that SN 2006X appears as the discrepant case in all of these fits, and that it always displays a polarization too high in comparison with the value that the correlation of the rest of the objects would suggest. The highly reddened SNe 2006X and 2014J appear to be indicative of the range of expected polarization values given a reddening.

Regarding the color excesses, Figure 11 repeats the message in Figure 9. The sodium sample shows a correlation between color excess and polarization when SN 2006X is excluded. Serkowski et al. (1975), Whittet & van Breda (1978), and Clayton & Mathis (1988), among other authors, have studied correlations between the color excess and $P_{\rm max}$ of Milky Way stars. With the exception of SN 2006X (see Patat et al. 2015), we cannot provide a reliable measurement of $P_{\rm max}$ for our SNe since it typically falls at the blue edge of our spectra or beyond. If we assume an average $\lambda_{\rm max} = 0.35\,\mu$m for most of the sample, the good match between Equations (1) and (3) implies that $P_{\rm mean} \simeq 0.86 P_{\rm max}$. With this translation, we see that our observations follow the average relation found by Fosalba et al. (2002) in their statistical study of polarized and reddened stars in the Milky Way (see in particular their Equation (3)). Also, a noted result from Serkowski et al. (1975) is that for a given color excess, there is a limit to the amount of polarization that the dust can imprint. This is given by the inequality $P_{\rm max} \leqslant 9.0E(B-V)$. This limit, translated to $P_{\rm mean}$, has been plotted in Figure 11 with a magenta solid line. The figure shows that all the SNe with $E(B-V) \gtrsim 0.1$, including our discrepant highly polarized SN 2006X, are well below the Galactic upper limit. According to the standards of polarized stars in the Milky Way, SNe Ia display modest polarization levels given their color excesses.

The correlation between $P_{\rm mean}$ and A_V shown in Figure 10 replicates in part the correlation that the former has with $E(B-V)$. In this case, the correlation is good both with and without SN 2006X but improves when it is removed from the fit. Again, SN 2006X appears as too highly polarized for the given extinction. If a value of R_V is assumed, Serkowski's upper limit of polarization for a given color excess can be transformed to an upper limit for a given extinction. To guide the eye, we have plotted the upper limit given by $P_{\rm mean} \leqslant 2.5A_V$, assuming $R_V \sim 3.1$. As shown in Figure 10, some SNe exceed this limit, indicating that the assumed value of R_V is larger than the actual value appropriate for the SNe. An $R_V \sim 2.0$ is a better upper limit to Figure 10, and it also agrees better with photometric studies of large SN Ia samples that tend to find values of R_V smaller than those typical of the Milky Way (Wang 2005; Goobar 2008; Folatelli et al. 2010; Burns et al. 2014).

In general, the comparison of Figures 9–11 with Figure 9 of Serkowski et al. (1975) suggests that our SNe display a noisy correlation. The dispersion in polarization increases with polarization so that the points scatter in a wedge. There appear to be upper and lower boundaries between polarization, color, color excess, or extinction, rather than an upper limit for the polarization for a given color, color excess, or extinction, especially for those objects with $E(B-V) \gtrsim 0.2$. This indicates that the efficiency of dust alignment is similar in the foreground regions of these SNe, particularly at moderate and low-extinction sight lines.

Spectropolarimetry can also enrich the discussion on the value of R_V through its connection with $\lambda_{\rm max}$. Many previous studies have suggested that the value of R_V measured for SNe Ia is generally smaller than the typical value, ~3, of our Galaxy and our spectropolarimetry is qualitatively consistent with them. We have plotted in Figure 13 the values of R_V expected from the relation $R_V/\lambda_{\rm max} \sim 5.5$ found by Serkowski et al. (1975) for the Milky Way (see the black stars). For fixed K, $\lambda_{\rm max}$ essentially determines the slope of the Serkowski law (Equation (1)) in the wavelength range used to fit Equation (3), and hence the slope b of our fitted straight line. In Figure 2, we distinguish three groups of foreground polarization slopes: $b \lesssim 0$, $b \sim 0$, and $b \gtrsim 0$. They are a consequence of the three ranges of $\lambda_{\rm max}$ mentioned earlier for the 12 SNe in the sodium sample ($\lambda_{\rm max} \sim 0.20$–$0.36\ \mu$m for eight SNe, ~0.50–0.55 μm for three of them, and ~0.75 μm for the remaining one), which, in turn, imply $R_V \sim 1.8$, 2.8, and 3.9, respectively. Although the values of R_V suggested by the observed polarization are qualitatively consistent with the values estimated from photometric observations, the quantitative differences could be an indication that the relation $R_V \sim 5.5\lambda_{\rm max}$ does not apply to the foreground polarizing dust of these SNe Ia host galaxies.

The polarimetric measurements suggest that a relevant fraction of the foreground dust in all of the SNe of the sodium sample is located in a fairly stable environment that has had time to relax. Turbulent or shocked regions will not permit a correlation between color excess and polarization. The polarizing dusty regions cannot be close to star-forming regions, nor to a circumstellar region produced by a recent episode of mass ejection by the SN progenitors, nor to the CSM shocked by the SN ejecta. The previous conclusion rules out a polarization imprinted by a local CSM. This has been confirmed in the case of SN 2014J by high-resolution spectroscopic studies by Maeda et al. (2016), who find that the sodium absorption systems originate in interstellar scales.

Still, even if it is not in the CSM realm, the polarizing dust could be associated with the SNe or their progenitors. Studies of polarization of transmitted light in stars where at least part of the foreground matter can be seen, as in reflection nebulae, show that when the nebulae appear relaxed, they display well-ordered physical structures, generally regularly spaced and approximately parallel filaments, which are also parallel to the polarization pseudo-vectors that trace the global Galactic structures. This indicates that there are regions, which could be called distant CSM, which are already threaded by the global magnetic field (Hall & Serkowski 1963; Spitzer 1968; Marraco & Clocchiatti 1988). The required condition is that the dusty gas stays under the influence of the global magnetic field for a time longer than the timescale for dust alignment, $\tau_{\rm DA}$. According to Draine & Weingartner (1997) this timescale is of the order $2 \times 10^5 \lesssim \tau_{\rm DA} \lesssim 1 \times 10^7$ years.

4.3. Polarization and Foreground Interstellar Absorption Lines

Sternberg et al. (2011) studied the velocity structure of the Na I D systems in 35 SNe Ia and categorized them into three classes: blueshifted when they display a dominant feature with one or more minor components at shorter wavelengths; redshifted when the minor components appear at longer wavelengths from the dominant feature; and single/symmetric when there is a single feature, or a system of lines symmetrically centered at the expected velocity of the SN host.[14] They find a statistically significant excess of blueshifted Na I D systems in the foreground matter of SNe Ia and interpreted this as evidence of outflows from the SN progenitors. Seven of our twelve SNe are included in their sample: SNe 2006X, 2008fp, 2007le, 2002bo, and 2007fb are blueshifted; SN 2010ev has a single absorption feature; and SN 2007af is redshifted. In order of strength of polarization signal (c.f. Figure 2), the blueshifted SNe are among the highest polarization (with the exception of SN 2007fb), the single symmetric one is in the middle, and the redshifted one near the bottom, at low polarization values.

Phillips et al. (2013) found that the SNe Ia that displayed foreground Na I D lines had a variety of proportions of sodium column density and A_V (i.e., different dust-to-gas ratios). Most of them would approach the average ratio found for the Milky Way, but about a third of their sample showed anomalously large Na I D column densities compared with the Milky Way ratio. The majority of these SNe with anomalously strong Na I D absorption are blueshifted, according to Sternberg et al. (2011).

In our Figure 12, the EWs of the Na I D and Ca II H and K foreground absorption lines show a generally similar trend with polarization, although the correlation is not as good as those between the polarization and color, color excess, or extinction, as discussed previously. Qualitatively, the two panels in Figure 12 repeat what Phillips et al. (2013) found for the correlation between A_V and the column densities of sodium and potassium. Since our sample is relatively small, we refrain from defining a region of average or normal values of EW for a

[14] We note that in the single case, it is really impossible to establish a Doppler shift for the line, since there is no main component to adopt as the rest frame. It is not possible to establish whether the single Na feature is shifted or not.

given $P_{\rm mean}$ and measure departures from those normal values as excess. The plots can, nevertheless, be interpreted as a correlation where the observed EWs of the Na I D or Ca II H and K lines fall within a range with upper and lower limits, which diverge from the mean as $P_{\rm mean}$ increases (a wedge-like scatter plot).

Our observations can be understood by assuming that the dominant source of polarization and extinction in the foreground of these SNe consists of a few regions of gas and dust, permeated by the same large-scale magnetic field, where a significant fraction of the dust has a smaller average size than is typical in the Milky Way. The regions could be close to the SN, in what we may call distant CSM, but the dominant part of the foreground matter is not in what is usually understood as CSM, under the direct mechanical or radiative influence of the SN explosion. It is reasonable to expect that, if not perturbed, this mix of dust and gas regions will evolve toward an equilibrium-like state, with a fairly well-defined dust-to-gas ratio. These average ratios give rise to the mean correlation between gas column density and A_V in the Milky Way and other galaxies, found by Sembach et al. (1993) and Phillips et al. (2013). In some of the sight lines toward our SNe Ia, however, the equilibrium-like stage has either not been reached or has been perturbed, resulting in a relative excess of Na I gas with respect to dust. A scenario like this would explain the enhanced strength of the Na I D lines in some SNe given their polarization (as in Figure 12) or their A_V (as in Phillips et al. 2013).

Where is the polarizing dust? It could be anywhere along the light path, although the correlations between polarization, reddening, and EW at the redshift of the parent galaxy mean that a major fraction is within the SN host galaxies. In the context of Sternberg et al. (2011), it is tempting to imagine the dust close enough to the SNe so as to connect their progenitors to the presence of, excess of, and/or blueshift in the Na I D absorption lines, but it cannot be very close to the SNe because the grains would be evaporated by the UV radiation.

As mentioned earlier, a small percentage of SNe Ia show variability in the EW of the Na I D lines (SNe 1999cl, 2006X, and 2007le; Blondin et al. 2009; Patat et al. 2009; Simon et al. 2009, respectively). This indicates that some of the CSM responsible for the Na I D absorption is actually within the radiative influence of the SN explosion. The cases of SNe 2006X and 2007le, which were studied at high resolution, reveal that the variable Na I D components imply a small fraction of the total EW. This fact, together with the constancy of continuum polarization in time and the realization that these SNe generally follow the same trends as the others in the correlations shown in Figures 8–13, lead us to conclude that the variable Na I D components are associated with polarizing dust.

Matter in the line of sight toward three events in our sample has been detected through light echoes (LEs). Wang et al. (2008) report the discovery of an LE in SN 2006X detected approximately 300 days after maximum light. They locate the reflecting dust between 27 and 170 pc from the SN, and also propose the existence of a second, inner, LE. Crotts & Yourdon (2008), using observations 680 days after maximum light, confirm the more distant LE, constraining its distance to 26 pc, and rule out the possibility of the inner one. In addition, they claim that the reflecting dust structure is the dominant source of extinction in SN 2006X. Drozdov et al. (2015) report two LEs in SN 2007af discovered in data taken three years after maximum light. There is a main outer echo located at ∼790 pc and produced by a foreground dust sheet, which should also dominate the extinction. The second, inner LE would be between 0.45 and 90 pc, depending on whether the dust is in front of or behind the SN. Crotts (2015) reports the detection of an LE from SN 2014J at 300 pc and a possible inner one at 80 pc from the SN. Finally, Yang et al. (2015) use *HST* observations ∼277 and ∼416 days after *B* maximum light to show that SN 2014J develops LEs from CSM located at foreground distances of ∼222 and ∼367 pc, with small-scale structures reaching down to approximately 1 pc. They also point out that the amount of dusty material involved in the echoes is much smaller than that involved in the total extinction. In all cases, the echos are bluer than the SNe, indicating high scattering efficiency at short wavelengths. This relates to a small average dust grain size, in agreement with our observations of small $\lambda_{\rm max}$. It is difficult to associate the presence of LEs in SNe 2006X and 2014J with other obvious peculiarities in their polarization. They are two of the most reddened and polarized SNe of the sodium sample but follow the general trends of the rest. The case of SN 2007af is different. It is one of the SNe with the lowest polarization, the angle of polarization is not aligned with major features of the parent galaxy, and the wavelength of maximum polarization is the longest of the sample. Drozdov et al. (2015) found evidence for two LEs. One of them, the outer echo, is located some 790 pc from the SN, in the foreground. The measured optical depth suggests that the dust in it is responsible for most of the extinction of the SN light curves, and, hence, it should also dominate the ISP. The dust responsible for the other, inner, echo is closer to the SN but its location could not be unambiguously determined. It could be ∼90 pc in the foreground, or 0.45 pc in the background. Even at the closest distance, the delay between the scattered light and direct light is far longer than the range of epochs at which we observed the SN. We conclude that the matter causing the LEs in SN 2007af is not responsible for polarizing the light at early times.

Could matter from the SN progenitors be at distances comparable to those inferred from the LEs *and* polarize light? The timescale for alignment of the dust in the magnetic field allows us to put some constraints, albeit weak, on the location. The dust has to be in a fairly relaxed region, far from strong shocks, strong winds, or other large-scale hydrodynamic phenomena, and it must have remained in this unperturbed state for a time longer than $\tau_{\rm DA}$. In the SD scenario, the dust could have originated in the winds of an evolved companion. At the typical velocity of 100 km s^{-1}, the smallest $\tau_{\rm DA}$ given by Draine & Weingartner (1997), 2×10^5 years, will put the matter at some 20 pc from the progenitor. Another limit comes from the constancy in time of the foreground polarization. Taking the longest time period covered by spectropolarimetric observations of an SN in our sample, seven weeks in the case of SN 2006X, as representative of the sample and 2×10^4 km s^{-1} as a typical maximum expansion velocity of SN ejecta means that the dust has to be farther than ∼0.1 pc in order to be safe from the ejecta colliding with it. Winds from the progenitor expanding during times as long as $\tau_{\rm DA}$, or longer, could put matter with the potential to provide aligned dust at a safe distance from the SN explosion, but it will not be close enough to be called CSM. The numbers are within the range of possibilities for the LEs observed but are only marginally

consistent with the scenario proposed by Soker (2014), where the foreground matter causing the enhanced Na I D lines has to be at distances of $\sim 10^{18}$ cm (0.32 pc) for the light of the SN to cause desorption of sodium atoms from the dust grains.

Why are the galactic environments in the foreground of the SNe with host Na I D lines in absorption systematically different from what we see in similarly reddened stars in the Galaxy? Why do they show more efficiency in polarizing blue light than those toward SNe that do not display these narrow lines? It may be relevant to note that there are lines of sight in our galaxy that show a relative increase of polarization in ultraviolet wavelengths. Martin et al. (1999) studied 28 lines of sight using *HST* data and report that two of them have an unusually short $\lambda_{\max}$. They claimed that the maximum polarization is high but the polarization efficiency is low, and remarked that these two sight lines lie in regions of active star formation, where there is evidence of stellar winds and supernova activity. They claimed that the statistical relevance of these two cases is small, and attributed the difference to variations in the dust grain shapes and/or efficiency in grain alignment. In our region of the Galaxy, short $\lambda_{\max}$ is the exception, not the norm (Patat et al. 2015).

It is tempting to surmise that the same process that produces an excess of sodium gas produces the polarization spectrum with short $\lambda_{\max}$. A scenario proposed by Hoang (2015) carries the promise of accounting for the contrasting elements of order and chaos revealed by Figures 7–13, and the results of Sternberg et al. (2011) and Phillips et al. (2013). Hoang's study of the dust grain size distribution and alignment in the foreground of SNe 2006X, 2008fp, 2014J, and 1986G finds that reproducing the small values of R_V requires both an increased total mass of small grains and efficiency in their alignment. He suggests that these SNe had matter located at distances much greater than the sublimation radius of the grains, but close enough that the radiation pressure from the SN light accelerates the dust clouds that are closer and makes them collide with those that are farther. The collisions alter the grain size distribution and bias them toward small sizes, while the radiative torques induced by the SN radiation promote a faster alignment, especially of the small grains. He finds that the relevant distance scales for these processes to work are 1–20 pc while the timescales for alignment can be as short as a few days. A scenario like this will also explain an increase in the gaseous phase of those atoms like sodium, which are generally more difficult to incorporate in the solid phase of the ISM and more sensitive to photodesorption (Draine 2004), and will also result in a preponderance of blueshifted Na I D line systems. The SNe that Hoang (2015) focused on are the four most polarized of our sodium sample. The rest of the SNe in the sodium sample could differ just in the amount of total ISM mass within the first $\sim$20 pc or whether there are different clouds that can be differentially accelerated. A critique of this scenario will argue that in cases like SN 2014J, high-resolution spectra reveal the presence of many individual Na I components (10, according to Maeda et al. 2016), which would be associated with different dusty regions at different distances from the SN, with many of them probably very distant. It is, then, neccesary to explain why those that are closer to the SN are the ones that dominate the polarization. Another issue to raise in the scenario of Hoang (2015) is that ISPs with Serkowski-like polarization and small $\lambda_{\max}$ are not typically observed in the lines of sight toward extragalactic core-collapse SNe. The general case for them is an ISP that is well-fitted by a Serkowski law with standard Galactic parameters (Leonard & Filippenko 2001; Leonard et al. 2002; Maund et al. 2007; Chornock et al. 2011). It will be also necessary, then, to explain why the radiation pressure from an SN causes such different effects in the environments of Type Ia and core-collapse SNe.

An estimate of the physical conditions in the regions where the foreground Na I D, K I, and Ca II lines are formed will certainly help to better constrain their location and provide firmer grounds for understanding. Environmental tests, like the Routly–Spitzer effect (Routly & Spitzer 1952), will be an appropriate tool. We cannot apply it to our data set because it requires column densities of the absorbing species, a piece of data that we cannot reliably estimate from our low-resolution spectra.

5. Conclusions

We have presented observations of the continuum polarization in the wavelength range from 420 to 580 nm of the 19 SNe Ia in our database that were observed at least twice, with one observation close to the time of maximum light. We have found that the presence of narrow Na I D lines of foreground origin at the redshift of the parent galaxies is connected with special characteristics of the polarization in this blue wavelength range. This led us to split the SNe into a sodium sample, which shows the lines, and a non-sodium sample, which does not.

The continuum polarization of the sodium sample (see Figure 2) is generally well-matched by the original ISP polarization spectrum found by Serkowski et al. (1975), with constant $K \simeq 1.15$ and values of $\lambda_{\max}$ that are short by the standards of the Galaxy. Furthermore, the blue continuum polarization is poorly fitted if the K versus $\lambda_{\max}$ relation found by Whittet et al. (1992) is used. For each SNe, the polarization remains approximately constant for the entire period of observation, which may be as long as several weeks. This rules out polarization originating in circumstellar LE, which should evolve on shorter timescales (Wang 2005; Patat et al. 2006). On the other hand, the non-sodium sample (Figure 3) typically shows smaller values of blue polarization and a wavelength dependence that can be well-fitted by a Serkowski profile with values of $\lambda_{\max}$ similar to those of the Galaxy, which follow the Whittet et al. (1992) relation. Additionally, the polarization pseudo-vectors of the sodium sample tend to align with the major macroscopic features of the parent galaxies while those of the non-sodium sample do not.

In the wavelength range 420–580 nm, where polarization intrinsic to the SNe is expected to be small, the foreground polarization can be reasonably well-described by $P_{\rm cont}(\lambda) = a + b\lambda$ (Equation (3)). There is a good correlation between b and $P_{\rm mean}$, the mean polarization in the selected blue wavelength range, which is expected for a Serkowski-type polarization. This makes it possible to describe the blue continuum polarization with a single observational parameter.

There are good correlations between $P_{\rm mean}$ and the color, color excess, and A_V of the SNe. They appear like the usual "wedge" scatter plots where the dispersion around the mean of the variable taken to be dependent grows together with the variable taken to be independent ($P_{\rm mean}$ in this case). A noisier relation also exists between $P_{\rm mean}$ and the value of R_V estimated from photometry. The latter is consistent with both extinction and polarization resulting from dust with a typical size smaller than the characteristic size of polarizing dust in our

neighborhood of the Galaxy. A correlation also exists between $P_{\rm mean}$ and the EWs of the foreground Na I D and Ca II H and K narrow lines, which can be also interpreted as upper and lower limits for $P_{\rm mean}$, given a column density of gas. As is typical of wedge-like scatter plots, these upper and lower limits are quite similar for small polarization, but they diverge to a large extent at higher polarizations.

The spectropolarimetric observations bring an additional element into the discussion of the location of the matter that reddens and/or polarizes the SN light. The polarizing dust has to be aligned with the magnetic field and so has to be in regions that have remained free from shocks, strong winds, or other large-scale hydrodynamic phenomena for times longer than the timescale for dust alignment. This rules out a polarizing dust located very close to the SN as in a CSM region. Still, the fact that the SNe with higher foreground continuum polarization are all blueshifted in the classification of Sternberg et al. (2011) would suggest that the relevant polarizing regions could be associated with the SN progenitor or the star-forming episode that gave birth to them. Since we cannot establish the distance between the polarizing dust and the SNe, however, our observations cannot be used to discern between the major scenarios for Type Ia SN progenitors and may be consistent with both of them.

Even though our sample is still small, there are two practical conclusions that follow from this study. One is that the presence of narrow Na I D lines at the redshift of the host galaxies, in SNe Ia, is an indirect indicator of the presence of dust grains, which have been shown to produce smaller $\lambda_{\rm max}$ values than those of the Milky Way. Hence, its presence is also an indicator of $R_V \lesssim 3$. In this case, Na I D lines at the redshift of the parent galaxy should be taken as an independent prior on R_V when simultaneously fitting light curves, *K*-corrections, and reddening for SNe Ia, especially for those used in cosmology. The other conclusion is that the presence of foreground Na I D lines at the redshift of the host impairs the possibility of assuming that the foreground ISP is "normal" in the sense of behaving like the ISP of the Galaxy. This should be taken as a warning sign on the prospects of studying the intrinsic continuum polarization of SNe Ia. Disentangling foreground and intrinsic polarization is, and will continue to be, a risky step. If the hypothesis that the foreground ISP is well-represented by a normal Serkowski law cannot be made, the only chance of reliably measuring it is through late-time polarization spectra with very good S/N ratio (like in Patat et al. 2009). Studies of intrinsic continuum polarization of Type Ia SNe should be restricted to those that do not show Na I D lines at the redshifts of their hosts, or to those that show sodium but have an extended time coverage since maximum light (more than 60 days).

Our results indicate that the light paths toward extragalactic SNe that show Na I D absorption caused by matter in the host galaxies display a peculiar polarization spectrum. SNe 2006X, 2008fp, and 2014J (Patat et al. 2015) appear as extreme, highly polarized, cases of a distribution that extends toward low polarizations as well. The simplest interpretation is that the lines of sight toward these events preferentially contain dust with different properties than the dust in the typical line of sight toward stars in the Galaxy. A scenario of nearby dust clouds accelerated by radiation pressure from the SNe and colliding with more distant ones (Hoang 2015) appears to contain many of the elements required to account for the observations, although there are still questions to answer to make it fully convincing.

A better data set to study the properties of these dusty regions should include high-resolution spectroscopy of the Na I D, K I, and Ca II lines, as well as some of the Diffuse Interstellar bands (DIBs), both from the parent galaxies and our Milky Way. The EW of DIBs is the most accurate tool to probe SN extinction according to Phillips et al. (2013). The K I lines would be especially important since they are less affected by saturation. The ideal data set should also include a very late spectropolarimetric observation, taken around 50 days after maximum light, like the ones we have for SNe 2006X and 2007le. These data sets would allow an estimate of the temperatures and densities of the dusty gas and help better understand whether the dust is related to the SNe or to their progenitors, or at least to confirm whether it is under the influence of the SN radiation. Better data sets also mean, plainly, improved statistics. We need more SNe observed in different types of galaxies since the global dust properties are expected to be related to the evolutionary stage of the hosts. Better observations will allow us, eventually, to bridge the gap between studying the foreground matter in SNe Ia and connecting the foreground, or parts of it, to a particular SN progenitor scenario.

We would like to thank Chris Burns and Mark Phillips for their very helpful data calculations and rich discussion. This paper is based on observations made with ESO Telescopes at the Paranal Observatory under the programs 068.D-0571(A), 069.D-0438(A), 070.D-0111(A), 076.D-0178(A), 079.D-0090(A), 080.D-0108(A), 081.D-0558(A), 085.D-0731(A), and 086.D-0262(A). Also based on observations collected at the German-Spanish Astronomical Center, Calar Alto (Spain).

Support for P.Z., F.F., S.G., and A.C. is provided by the Ministry of Economy, Development, and Tourism's Millennium Science Initiative through grant IC120009, awarded to The Millennium Institute of Astrophysics, MAS, and by CONICYT through grant Basal CATA PFB 06/09. The research of J.R.M. is funded through a Royal Society University Research Fellowship. The research of J.C.W. was supported in part by NSF grant AST-1109801.

Appendix
SN 1986G

We have included a publicly available spectrum of SN 1986G near maximum light[15] which also has polarimetric data published by Hough et al. (1987).

This is a highly polarized SN Ia with large amounts of sodium in its host, Centaurus A. Although the observations are not spectropolarimetric, they make a good addition to our sample. Different filters used by Hough et al. (1987) allow us to model the Serkowski law in the same way as our spectropolarimetric sample, but with a much larger error (see Figure 14). We obtain $\lambda_{\rm max} = 0.43$ μm and for the linear fit $P_{\rm mean} = 4.98 \pm 1.73$ and $b = -0.003 \pm 0.001$. As most of the highly polarized and sodium rich SNe in our sample, SN1986G also shows a polarization angle aligned with the disk structure of its host (see Figure 15).

Extinction values were obtained from Phillips et al. (2013), where $A_V = 2.03 \pm 0.11$ and $(B - V)_{\rm Bmax} = 1.08 \pm 0.5$

[15] From Weizmann Interactive Supernova data REPository (WISeREP), http://wiserep.weizmann.ac.il/.

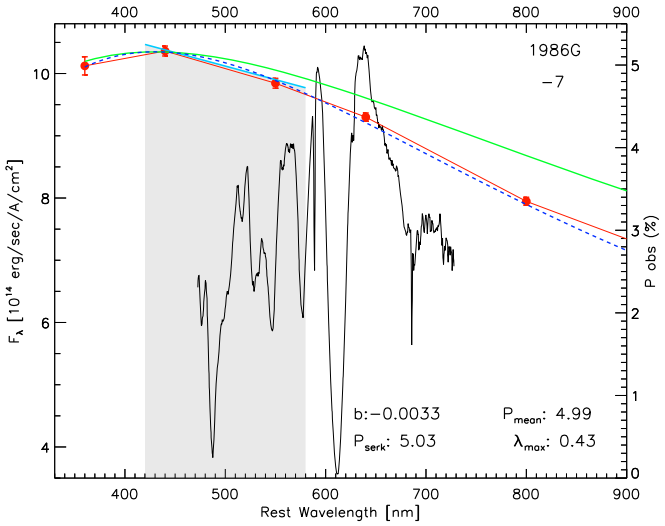

Figure 14. Same as Figure 2, except for imaging polarimetry data of SN 1986G acquired by Hough et al. (1987).

Figure 15. Same as Figure 5 for SN 1986G in Centaurus A.

mag. The color excess corresponds to an average value $E(B-V) = 1.09 \pm 0.43$ mag from the calculations of Hough et al. (1987) and Phillips et al. (1987, 2013).

For the EWs of Na I D and Ca II H and K, Phillips et al. (1987) measures 3.6 and 1.75 Å, respectively, while D'Odorico et al. (1989) find 4.53 and 2.45 Å. We take the average between these two and consider equivalents widths of 4.07 ± 0.66 and 2.10 ± 0.49, respectively.

References

Amanullah, R., Goobar, A., Johansson, J., et al. 2014, ApJL, 788, L21
Appenzeller, I., Fricke, K., Fürtig, W., et al. 1998, Msngr, 94, 1
Benetti, S., Meikle, P., Stehle, M., et al. 2004, MNRAS, 348, 261
Blondin, S., Matheson, T., Kirshner, R. P., et al. 2012, AJ, 143, 126
Blondin, S., Prieto, J. L., Patat, F., et al. 2009, ApJ, 693, 207
Burkey, M. T., Reynolds, S. P., Borkowski, K. J., & Blondin, J. M. 2013, ApJ, 764, 63
Burns, C. R., Stritzinger, M., Phillips, M. M., et al. 2014, ApJ, 789, 32
Chornock, R., Filippenko, A. V., Branch, D., et al. 2006, PASP, 118, 722
Chornock, R., Filippenko, A. V., Li, W., et al. 2011, ApJ, 739, 41
Clayton, G. C., & Mathis, J. S. 1988, ApJ, 327, 911
Cox, N. L. J., & Patat, F. 2014, A&A, 565, A61
Crotts, A. 2015, ApJL, 804, L37
Crotts, A. P. S., & Yourdon, D. 2008, ApJ, 689, 1186
Davis, L., Jr., & Greenstein, J. L. 1951, ApJ, 114, 206
D'Odorico, S., di Serego Alighieri, S., Pettini, M., et al. 1989, A&A, 215, 21
Draine, B. T. 2004, in Saas-Fee Advanced Course 32: The Cold Universe, ed. D. Pfenniger & Y. Ravez (Berlin: Springer), 213
Draine, B. T., & Weingartner, J. C. 1997, ApJ, 480, 633
Drozdov, D., Leising, M. D., Milne, P. A., et al. 2015, ApJ, 805, 71
Folatelli, G., Morrell, N., Phillips, M. M., et al. 2013, ApJ, 773, 53
Folatelli, G., Phillips, M. M., Burns, C. R., et al. 2010, AJ, 139, 120
Förster, F., González-Gaitán, S., Anderson, J., et al. 2012, ApJL, 754, L21
Fosalba, P., Lazarian, A., Prunet, S., & Tauber, J. A. 2002, ApJ, 564, 762
Ganeshalingam, M., Li, W., Filippenko, A. V., et al. 2010, ApJS, 190, 418
Goobar, A. 2008, ApJL, 686, L103
Gutiérrez, C., Folatelli, G., Pignata, G., Hamuy, M., & Taubenberger, S. 2011, BAAA, 54, 109
Hall, J. S., & Serkowski, K. 1963, in Stars and Stellar Systems, Vol. 3, ed. K A. Strand (Chicago, IL: Univ. Chicago Press), 293
Hicken, M., Challis, P., Jha, S., et al. 2009, ApJ, 700, 331
Hoang, T. 2015, ApJ, in press (arXiv:1510.01822)
Hough, J. H., Bailey, J. A., Rouse, M. F., & Whittet, D. C. B. 1987, MNRAS, 227, 1
Howell, D. A., Höflich, P., Wang, L., & Wheeler, J. C. 2001, ApJ, 556, 302
Iben, I., Jr., & Tutukov, A. V. 1984, ApJS, 54, 335
Iben, I., Jr., & Tutukov, A. V. 1996, ApJS, 105, 145
Krisciunas, K., Suntzeff, N. B., Phillips, M. M., et al. 2004, AJ, 128, 3034
Landolt, A. U. 1992, AJ, 104, 372
Leonard, D. C., & Filippenko, A. V. 2001, PASP, 113, 920
Leonard, D. C., Filippenko, A. V., Barth, A. J., & Matheson, T. 2000, ApJ, 536, 239
Leonard, D. C., Filippenko, A. V., Chornock, R., & Li, W. 2002, AJ, 124, 2506
Leonard, D. C., Li, W., Filippenko, A. V., Foley, R. J., & Chornock, R. 2005, ApJ, 632, 450
Li, W., Bloom, J. S., Podsiadlowski, P., et al. 2011, Natur, 480, 348
Li, W., Filippenko, A. V., Chornock, R., et al. 2003, PASP, 115, 453
Maeda, K., Tajitsu, A., Kawabata, K. S., et al. 2016, ApJ, 816, 57
Maguire, K., Sullivan, M., Patat, F., et al. 2013, MNRAS, 436, 222
Marion, G. H., Brown, P. J., Vinkó, J., et al. 2016, ApJ, 820, 92
Marion, G. H., Sand, D. J., Hsiao, E. Y., et al. 2015, ApJ, 798, 39
Marraco, H. G., & Clocchiatti, A. 1988, LNP, 315, 120
Martin, P. G., Clayton, G. C., & Wolff, M. J. 1999, ApJ, 510, 905
Mathewson, D. S., & Ford, V. L. 1970, MNRAS, 74, 139
Maund, J. R., Wheeler, J. C., Patat, F., et al. 2007, A&A, 475, L1
Maund, J. R., Wheeler, J. C., Wang, L., et al. 2010, ApJ, 722, 1162
Nomoto, K. 1982, ApJ, 253, 798
Pakmor, R., Kromer, M., Taubenberger, S., et al. 2012, ApJL, 747, L10
Patat, F., Baade, D., Höflich, P., et al. 2009, A&A, 508, 229
Patat, F., Benetti, S., Cappellaro, E., & Turatto, M. 2006, MNRAS, 369, 1949
Patat, F., Höflich, P., Baade, D., et al. 2012, A&A, 545, A7
Patat, F., Maund, J. R., Benetti, S., et al. 2010, A&A, 510, 108
Patat, F., & Romaniello, M. 2006, PASP, 118, 146
Patat, F., Taubenberger, S., Cox, N. L. J., et al. 2015, A&A, 577, A53
Patat, F., Taubenberger, S., Baade, D., et al. 2014, ATel, 5830
Phillips, M. M., Li, W., Frieman, J. A., et al. 2007, PASP, 119, 360
Phillips, M. M., Phillips, A. C., Heathcote, S. R., et al. 1987, PASP, 99, 592
Phillips, M. M., Simon, J. D., Morrell, N., et al. 2013, ApJ, 779, 38
Routly, P. M., & Spitzer, L., Jr. 1952, ApJ, 115, 227
Sahu, D. K., Tanaka, M., Anupama, G. C., et al. 2008, ApJ, 680, 580
Scarrott, S. M., Ward-Thompson, D., & Warren-Smith, R. F. 1987, MNRAS, 224, 299
Schlafly, E. F., & Finkbeiner, D. P. 2011, ApJ, 737, 103
Schlegel, D. J., Finkbeiner, D. P., & Davis, M. 1998, ApJ, 500, 525
Sembach, K. R., Danks, A. C., & Savage, B. D. 1993, A&AS, 100, 107
Serkowski, K., Mathewson, D. S., & Ford, V. L. 1975, ApJ, 196, 261
Simon, J. D., Gal-Yam, A., Gnat, O., et al. 2009, ApJ, 702, 1157
Soker, N. 2014, MNRAS, 444, L73

Spitzer, L., Jr. 1968, ITPA, 28, 262
Sternberg, A., Gal-Yam, A., Simon, J. D., et al. 2011, Sci, 333, 856
Wang, L. 2005, ApJL, 635, L33
Wang, L., Baade, D., Patat, F., & Wheeler, J. C. 2006, CBET, 396, 2
Wang, L., & Wheeler, J. C. 2008, ARA&A, 46, 433
Wang, L., Wheeler, J. C., & Hoeflich, P. 1997, ApJL, 476, L27
Wang, X., Filippenko, A. V., Ganeshalingam, M., et al. 2009, ApJL, 699, L139
Wang, X., Li, W., Filippenko, A. V., et al. 2008, ApJ, 677, 1060
Webbink, R. F. 1984, ApJ, 277, 355
Wheeler, J. C., & Hansen, C. J. 1971, Ap&SS, 11, 373
Whelan, J., & Iben, I., Jr. 1973, ApJ, 186, 1007
Whittet, D. C. B., Martin, P. G., Hough, J. H., et al. 1992, ApJ, 386, 562
Whittet, D. C. B., & van Breda, I. G. 1978, A&A, 66, 57
Yang, Y., Wang, L., Baade, D., et al. 2015, arXiv:1511.02495